INSTITUTO SUPERIOR DE ENGENHARIA DE LISBOA

Área Departamental de Engenharia Mecânica

ISEL

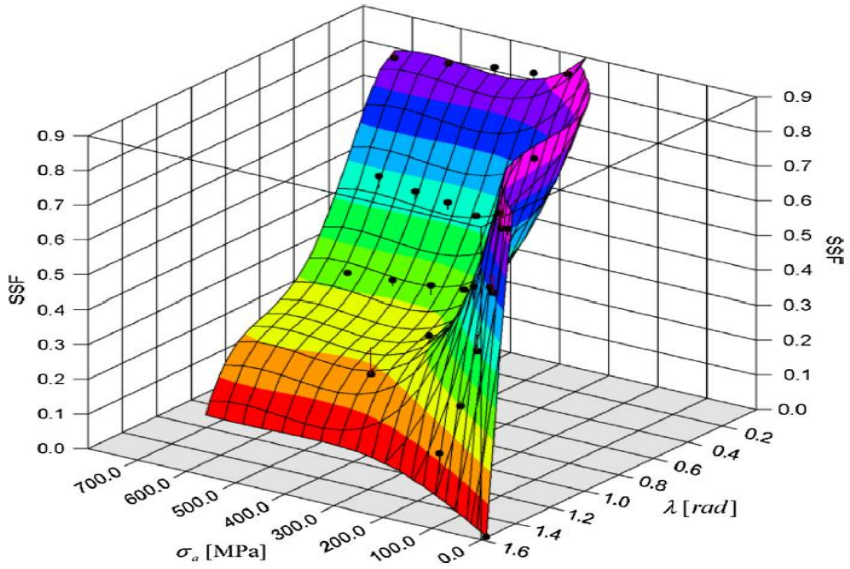

A Critical Review on Multiaxial Fatigue Models

FRANCISCO JOÃO BUMBA PACA
(Licenciado em Engenharia Mecânica)

Trabalho Final de Mestrado para obtenção do grau de Mestre
em Engenharia Mecânica

Orientador:
Prof. Doutor Vitor Manuel Rodrigues Anes

Júri:
Presidente: Prof. Doutora Maria Teresa Moura E Silva
Vogais: Prof. Doutor Luís Filipe Galrão dos Reis
Prof. Doutor Vitor Manuel Rodrigues Anes

Julho de 2021

INSTITUTO SUPERIOR DE ENGENHARIA DE LISBOA

Departamento de Engenharia Mecânica

ISEL

A Critical Review on Multiaxial Fatigue Models

FRANCISCO JOÃO BUMBA PACA
(Licenciado em Engenharia Mecânica)

Trabalho Final de Mestrado para obtenção do grau de Mestre
em Engenharia Mecânica

Orientador:
Prof. Doutor Vitor Manuel Rodrigues Anes

Júri:
Presidente: Prof. Doutora Maria Teresa Moura E Silva
Vogais: Prof. Doutor Luís Filipe Galrão dos Reis
Prof. Doutor Vitor Manuel Rodrigues Anes

Julho de 2021

“No great discovery was ever made without a bold guess”

ISAAC NEWTON

Acknowledgments

First and foremost, I would like to thank the Almighty God for the gift of life. I am tremendously happy to have Dr Vítor Anes as my supervisor. I am so grateful for his patience, availability and desire to always make things clear so that I could know what to do. During different stages of the dissertation, my supervisor always pushed for me and showed that things can always be improved, thank you very much Dr Anes.

I would extend my gratitude to all the professors I had during my two years at ISEL, I believe that each one of them played an important role in making this dissertation come into reality. I would also thank all my classmates specially Valdemar Rodriguez who welcomed me at ISEL as I was new student and showed me how things work there.

I would like to thank my parents João Bumba and Anastácia Maurício Bumba for unconditional love and support during my time in Portugal. My special thanks also go to my brothers, family, friends and to everyone who directly or indirectly was part of this achievements.

Lastly, I want to say thank you for everyone who encouraged me to never give up, to always continue dreaming and doing what is required to make my dreams become true.

Abstract

Most failures in structures mechanical components happen due to fracture and fatigue, which means that mechanical design engineers need to understand the physical phenomena behind these failures. An important aspect that remains to be fully understood is the influence of loading type on the materials fatigue strength. Proportional and nonproportional loads result in different fatigue lives, even when it is applied the same loading amplitudes in both loading conditions. Also, within proportional loads, it can be obtained different fatigue lives according to the ratio between shear and normal stresses. These aspects have been studied over the recent decades and many models have been proposed in literature to overcome these issues, however, a universal model to estimate fatigue strength of materials considering loading effects remains to be reached.

In this dissertation, a literature review was carried out focusing on multiaxial fatigue topics, i.e., the review started with the phenomenological characterization of fatigue, passing through critical plane models, cycle counting methods, and ending in fatigue damage monitoring. During the literature review, the stress scale factor (SSF) model, an equivalent shear stress model, raised relevant questions which were studied in the following chapters.

This study was conducted using multiaxial fatigue data of the high strength steel 42CrMo4 obtained from literature. These data were originally evaluated and computed at 0° for five multiaxial loading paths, and in this study the analysis was extended to other plane orientations starting from -90° to 90°. The research hypothesis was motivated by the existence of a plan whose orientation would simplify the assessment of the SSF damage map. The ultimate goal would be to estimate SSF damage map based on parameters obtained with simple tests. The actual method to determine the SSF damage map is based on Datafit, a commercial software that contains huge set of multivariable function used to perform regressions of experimental data. To facilitate the regression for a wide range of plane orientations an alternative method to determine the SSF damage map was developed to be later implement in a programming routine.

The findings obtained demonstrated that in fact the damage scale does vary with the plane orientation. With regard to the plane in which the damage map was evaluated, i.e., crack initiation plane at -16° obtained with PP45 loading path, the results demonstrated that a good fatigue life results can be estimated from another plane orientation rather than 0°. Moreover,

the results of the critical plane models estimate for the orientation of the crack initiation plane at -16° showed some good correlations except the SWT model.

Lastly, the new method developed to estimate the SSF damage map was used to estimate the SSF damage map in the plane oriented at -16°, the results obtained were not satisfactory when compared with the result obtained with the SSF damage map estimated using the commercial software Datafit. However, for 0° orientation, the proposed method yields a quite good SSF damage map which predicts fatigue life results better than those obtained using the SSF damage map obtained with Datafit at 0°.

Keywords: Multiaxial Fatigue, Critical Plane, Stress Scale Factor (SSF), Damage Parameter, Fatigue Life.

Resumo

Durante o século 21 várias catástrofes aconteceram envolvendo componentes mecânicos submetidos a determinados níveis de tensões. Essas catástrofes impulsionaram a investigação e o desenvolvimento de tecnologias mais avançadas de modos a garantir o bom funcionamento e a integridade dos componentes mecânicos durante o seu tempo de vida. De realçar que falhas nos componentes mecânicos causam vários prejuízos entre eles prejuízos económicos para empresas ou países, prejuízos ambientais e em muitas situações também podem ceifar vidas humanas, por esse motivo é de extrema importância que os engenheiros percebam o comportamento dos componentes mecânicos quando submetidos a tensões constantes ou cíclicas. Sabendo o comportamento mecânico dos materiais permite que os engenheiros ou outros especialistas envolvidos saibam com rigor quando determinado componente ou sistema precisa ser substituído ou precisa apenas de manutenção.

A maioria das falhas dos componentes mecânicos tem como causa principal a fadiga ou fratura, o que quer dizer que esses conceitos devem ser percebidos muito bem e também quer dizer que os engenheiros responsáveis pelo design dos componentes mecânicos devem considerar deformações plásticas em todas as fases do design isso porque muitos componentes falham por causa de determinadas características relacionadas ao design. Por exemplo, pontas afiadas, zonas com descontinuidade geométricas acentuadas, entalhes com zonas de grande concentração de tensão, o que pode contribuir para o aumento da possibilidade de o componente vir a falhar. Portanto, o conhecimento do comportamento dos componentes mecânicos quando submetidos a carregamentos de diferentes naturezas é de extrema importância para se saber quantificar com rigor o dano que o componente pode suportar evitando deste modo falha do mesmo componente.

Nesse trabalho foi realizada uma revisão da literatura concernente a fadiga multiaxial. Na revisão da literatura foram abordados aspetos como: noções fundamentais sobre fadiga, modelos do plano critico, métodos de contagem de ciclos, método de dano acumulado mais utilizado, a Regra de Miner, e previsão de vida á fadiga. Da revisão da literatura, o modelo de fadiga multiaxial Stress Scale Factor (SSF) foi utilizado para se explorar a existência de outros planos onde o mapa de dano SSF possa ser avaliado. Para finalizar modelo SSF foi utilizado para estimar a vida à fadiga usando mapa de dano SSF obtido no Datafit e o mapa de dano obtido por um método alternativo proposto nesta tese.

Para se efetuar esse estudo, resultados experimentais em fadiga do aço 42CrMo4 submetido a cinco diferentes carregamentos proporcionais nomeadamente tensão pura (PT), corte puro (PS), e três carregamentos proporcionais com diferentes amplitudes de tensão foram obtidos da literatura. Os resultados experimentais de fadiga obtidos da literatura foram avaliados para o plano 0°, com esse estudo pretende-se estender a análise para outros planos começando de -90° até 90°. Para cada um dos planos de -90° até 90° foi estimado a respetiva tensão normal e tensão de corte, com os valores das tensões estimadas juntamente com o carregamento de referência (corte puro) calculou-se o SSF para cada plano. Os valores estimados do parâmetro de dano SSF juntamente com as suas respetivas orientações foram representadas graficamente de modos a perceber o comportamento do parâmetro de dano SSF com a variação da orientação.

Da literatura obteve-se resultados experimentais da orientação do plano critico (-16°) do aço 42CrMo4 sujeito ao carregamento proporcional PP45. Nesse trabalhou, avaliou-se o mapa de dano SSF para orientação do plano critico (-16°) usando o software Datafit. Posteriormente os modelos do plano crítico (com uma tensão normal de 435MPa) foram utilizados para estimar o ângulo de iniciação de fenda e compará-los com resultado obtido da literatura. Para se identificar o ângulo do plano crítico, foi estimado o parâmetro de dano para cada plano começando de -90° até 90°, e finalmente o parâmetro de dano obtido para cada um dos modelos, nomeadamente SWT, Brown-Miller, Fatemi-Socie e Liu,foram representados graficamente juntamente com a respetivo plano.

Datafit possui uma base de dados com número elevado de funções usadas na regressão dos resultados experimentais de forma a obter o mapa de dano SSF, no entanto surge a dúvida de que possa haver uma outra função fora da base de dados do Datafit que possa levar a superficies de dano SSF mais fáceis de usar e com melhores estimativas, partindo desta hipótese o presente trabalho termina com a apresentação de uma metodologia alternativa ao Datafit para se determinar a superfície de dano SSF, esta metodologia alternativa usa polinómios do terceiro grau para modelar o SSF. A modelação SSF da metodologia proposta foi implementada usando Microsoft Excel.

Os resultados do parâmetro de dano SSF em relação a variação do respetivo plano de avaliação, demonstraram que de facto o parâmetro de dano varia com a variação do ângulo, sendo este resultado uma das causas que justificam os maus resultados dos modelos de previsão da vida à fadiga. Relativamente a superfície de dano correspondente a orientação do plano critico (-16°), foi possível obter um mapa de dano SSF com R^2 mais próximo de 1 do que o mapa de dano a 0° obtido da literatura, isso quer dizer que de facto existem outras

orientações possíveis de prever mapa de dano que representa bem o comportamento do fenómeno de fadiga e consequentemente estimam bons resultados de vida à fadiga. Quanto ao resultado obtido pelos modelos do plano critico, verificou-se que os modelos de fadiga multiaxial que são mais sensíveis iniciação dominada pelo corte, Fatemi-Socie e Brown-Miller, produziram bons resultados o que era expectável por causa do material utilizado, aço 42CrMo4 considerado um material dúctil cujo crescimento da fenda é dominado pelo corte. Com o modelo Liu, combinação de Liu1 e Liu2, também foi possível obter boa estimativa do ângulo de iniciação de fenda. Finalmente, o modelo SWT produziu ângulo do plano critico muito diferente do resultado experimental, o que também é esperado visto que o modelo SWT a iniciação é dominada pela tensão normal.

Finalmente, os resultados do mapa de dano SSF para a orientação do plano critico obtido usando a metodologia proposta apresentaram resultados não muito satisfatórios comparados com o mapa de dano SSF obtido a partir do Datafit. O mapa de dano SSF do método alternativo apresentou uma evolução que não corresponde com o fenómeno físico da fadiga. Mas, para 0° o mapa de dano SSF estimado a partir da metodologia proposta previu bons resultados quando comparado com o mapa de dano SSF obtido usando o Datafit para a mesma orientação. Relativamente à vida à fadiga usando o mapa de dano SSF a 0° obtido através metodologia proposta foi possível estimar melhores resultados do que usando mapa de dano SSF a 0° obtido pelo Datafit, com base neste resultado chegou-se a conclusão que podem existir outras funções fora da base de dados do Datafit que produzem melhores estimativas de vida à fadiga e que ao invés de dependermos de um software pago podemos obter boas estimavas do mapa de dano SSF usando a metodologia alternativa o que requer apenas bons conhecimento de Microsoft Excel. Com a realização desta dissertação foi possível verificar que usando o modelo de fadiga multiaxial SSF pode-se estimar bons resultados de vida à fadiga.

Palavras-chave: Fadiga Multiaxial, Stress Scale Factor (SSF), Modelos do Plano Crítico, Parâmetro de Dano, Vida à Fadiga.

Table of Contents

List of figures

List of tables

Nomenclature

σ_{max}	maximum normal stress
σ_{min}	minimum normal stress
$\Delta\sigma$	stress range
σ_m	normal mean stress
σ_a	normal stress amplitude
R	stress ratio
A	amplitude ratio
S_1, S_2, S_3, and S_4	stress points in three and four points method
ε_{eq}	equivalent strain
ε_x, ε_y and ε_z	strain components
γ_{xy} , γ_{yz} and γ_{xz}	shear strain components
ν	effective Poisson ratio
ν^e	poison elastic coefficient in Wang and Brown method
ν^p	poison plastic coefficient in Wang and Brown method
ε^e	elastic coefficient in Wang and Brown method
ε^p	plastic coefficient in Wang and Brown method
ε_{eq}^{rel}	relative equivalent strain
D	total damage
n_i	number of cycles
$\varepsilon_1, \varepsilon_2, \varepsilon_3$	principal strains
ε_n	normal strain
$\Delta\varepsilon_n$	shear strain range
$\Delta\gamma_{max}$	maximum shear strain range
S	normal strain coefficient
$\acute{\sigma_f}$	axial fatigue strength coefficient
$\sigma_{n,med}$	normal mean stress
$\acute{\varepsilon_f}$	axial fatigue ductility coefficient
b	axial fatigue strength exponent
c	axial fatigue ductility exponent
N_f	number of cycles to failure

E	Young's modulus,
$\sigma_{n,max}$	maximum normal stress
σ_y	yield stress
k	material constant
$\acute{\tau_f}$	shear fatigue strength coefficient.
G	shear modulus
$\acute{\gamma_f}$	shear fatigue ductility coefficient
b_γ	shear fatigue strength exponent
c_γ	shear fatigue ductility exponent
ε_a	maximum strain amplitude
$\Delta\tau$	shear stress range
ΔW	work
ΔW^e	elastic work
ΔW^p	plastic work
ΔW_I	axial work
ΔW_{II}	shear work
$\sqrt{3}\tau$	shear component of von Mises criterion
τ_{tresca}	shear equivalent stress of Tresca yield criterion
$\sigma_{x,global}(t)$	global stress component in x direction
$\sigma_{y,global}(t)$	global stress component in y direction
$\sigma_{\theta,local}(t)$	local stress
$\tau_{xy,global}$	global shear
$\tau_{xy,local}(t)$	local shear
SSF	stress scale factor
λ	stress amplitude ratio

1. Introduction

In the last two centuries many technological advances have been made in engineering. For instance, today it is possible to go faster from Europe to Africa using an airplane than it used to be a century ago. The advances made in transportation industry which is one of the key part in global economy/trading is very important because the economy is very dependent on products and services, it means that in order to delivery those products or services faster and cheaper the transportation industry must be efficient. So, achieving efficiency means that engineers must ensure the reliability as well as the functionality of each component.

When it comes to manufacturing in the transportation industry, there are several materials that can be used to manufacture a car, an airplane, a train, a helicopter, or any other means of transportation. The large number of materials available means that the process of selecting is much more complex because it will be dependent on many factors such as environmental condition, service restrictions, the amount of load it can withstand and so on. A new product is developed when there is a need to be satisfied. In engineering, the development of a new product starts with defining the product requirements, its functionality, specifications and also its expected lifetime.

Prior to the manufacturing, the component to be built is designed and then the design goes to the validation process. Engineering design is an iterative process in which all individual components and their requirements are at end analysed as whole and changes are made in the design process if necessary. The validation of a design is typically done by computational simulation together with prototype testing.

However, in all stages of the design process and validation it is very important to consider plastic deformation that may lead to failure due to the loading condition. This is important because the design features itself may increase the likelihood of a failure. For instance, it is known that sharp corners are areas of high stress concentration, this means that crack will tend to form in those areas. Therefore, designers should avoid sharp edges rather implement curved edges to minimise stress concentration and ultimately increase component life cycle.

Most key components used in transportation industry are made of metals which in service experience periodic changes in loads. Over time those variations in loads can cause failure of the component. When a component is manufactured, it is expected to perform a

specific task for a defined amount of time until it can be repaired or removed. However, many components fail before its expected life cycle and a failure of component may lead to many undesirable consequences such as damage to other components, the environment, loss of human lives, financial losses as well as cost for repairing or even replacing.

Over time new technologies have been introduced and the introduction of new technology means more challenges for people who are responsible for engineering design. The implementation of new technology may demand both more efficient use of material as well as improved material. When it comes to the economical aspect, fracture and deformation are considered to be problems of major importance, especially in the motor vehicle and aircraft sectors. In various sectors of the economy, the financial cost associated with avoiding fracture and the problem caused by it, it is nearly 4% of the gross national product (GNP) [1].

For instance, car body and bogie frame are typically designed to operate for more than 25 years [2]. It is possible for a fractured bogie frame to reduce the service life since the maximum stress is lower than the fatigue limit. However, the vast majority of failure of end beams are caused by fatigue [3].

According to Callister [4] approximately 90% of failures in mechanical components are due to fatigue. A research conducted by the National Institute of Standard and Technologies and Batelle Columbus Laboratories in the United states in 1983 [5] concluded that failures caused by fracture were estimated to cost $119 billion per year, which was approximately 4 percent of the country gross domestic product (GDP). According to the same research $35 billion would have been saved per year if advanced technologies were available and fatigue failure was properly understood and through more research in fracture that cost could be even more reduced by as much as $28 billion per year.

During the 20^{th} century many accidents caused by fatigue failure took place. For example, in 1954 commercial British aircraft named as de Havilland Comet failed at very high altitude causing many human losses and caused the British to lose the lead the in-transportation industry. The reason behind the accident was a rivet that was not properly punched into the aircraft during construction and because of that a microscopic manufacture defect was created due to pressurization systems that exert enormous strain on the fuselage causing stress to the skin especially around the window doors. Repeated pressure made the manufacture defect into fatigue crack which increases over time leading to a catastrophic failure.

The historical fatigue failure mentioned above, and many others made the scientific community to do further research in order to understand the reasons behind these accidents. This led to the revisiting of fracture mechanics theory developed by Erwin [6], which then

contributed to the better understanding of the material failure. For instance, the fact that a presence of crack in a material can change its local stress made the designing against fracture very challenging process.

The fracture mechanics theory is based on the assumption that there is an existing crack in a material which would increase over time until it becomes critical. The objective of this theory is to predict at which applied load will the crack length propagation be faster until it reaches a critical value. Using this theory in design stages, engineers must be able to estimate or measure the pre-existing cracks and determine their respective stress intensity factor to be correlated with the material fracture toughness. Knowing the initial crack in a material, engineers are able to monitor its behaviour before it reaches a critical point. According to Milne, using the fracture mechanics approach is the best way to manage structural integrity, this is because this theory has shown to be reliable for some high tech applications [7].

Many studies were done in the past in order to estimate how much fracture failure costs to the economy of advanced countries. Most of the financial loss due to fracture failure come from various factors including: direct repair or replacement costs; loss of revenue while unavailable; costs of finding replacement services or components to maintain business during unavailability; costs of consequential damage; consequential costs to avoid failure on similar items; total loss of business or public image; costs of otherwise unnecessary activities; costs of safety related issues, including insurance claims, litigation, loss of life [8].

Understanding the reason why some structures or components fail prior to their estimated lifetime is very important. Because it helps design engineers, to consider failure analysis in the early stages of the design by avoiding factors that can increase the probability of failure of a component. The understanding of failure mechanism also helps the maintenance technicians to identify signs of fatigue failure before it occurs.

1.1 Motivation

Despite of the developments in fracture mechanics theory, there is still a need to develop tools that are reliable and can be used in engineering application, this is because what is available today have some shortcomings. The tools must be able to correctly collect the information about damage accumulation under multiaxial loading and then this damage must be related with structure monitoring health. It is still a challenge to accurately describe and interpret, in terms of cumulative damage, the information that is collected from sensors.

It is known that most engineering components and structures in service experience multiaxial stress state with variable or random loading conditions. Nowadays, the real challenge is to find correlation between instrumentation, theoretical and the multiaxial model.

It is also important to mention that the cumulative damage model that are available today are still very basic and the existing cycle counting techniques many times cannot fully identify cycles from complex loading which means that they show low reliability in real time application. Furthermore, most of the cycle counting that are used today are based on the rainflow method which means that they all still carry the drawbacks associated with the rainflow technique.

1.2 Objectives

The objectives of this dissertation are:

- Perform a literature review about multiaxial fatigue, in order to understand what is currently known about multiaxial fatigue and what are the existing models and how those models deal with multiaxial stress state.
- Understand the stress scale factor (SSF) methodology in order to generate SSF damage map for different orientations.
- Propose an alternative approach to determine the SSF damage map without relying on a paid software.
- Propose future developments in order to improve the results of the alternative method.

1.3 Thesis outline

This dissertation is divided in four chapters, as follow:

In the first chapter, the reader is introduced to multiaxial fatigue importance to several industries which underlines the need to better understand fatigue and its impact on innovation of products, business and industry in general. This chapter ends with stating the dissertation motivation, objectives as well as its structure.

Chapter 2 begins with literature review focusing a brief development of fatigue failure theory. In this chapter, the basics of the fatigue and cycle loading description is provided. Then several uniaxial and multiaxial cycle counting are described, and their deficiencies are also underlined. This chapter also gives a background about some critical plane models that will be used in this dissertation and the SSF approach is introduced. In this section a description of

linear cumulative damage rule known as Miner rule is presented and it is highlighted why it is still widely used even though it shows some shortcomings. Finally, this chapter ends with a short description about fatigue life monitoring.

In chapter 3 experimental data obtained from literature will be used to compute SSF parameter for several other orientations rather than just one orientation as shown in the literature data. Based on SSF results for those orientation it will be shown how this damage parameter varies with plane orientation and fatigue life. A critical plane angle obtained from the literature will be used to determine the SSF parameter at that orientation and then perform regression using Datafit in order to obtain SSF surface at critical plane orientation which will be compared with the SSF surface at 0° degrees. In this chapter, for each critical plane models described previous chapter a graph is presented so that the damage parameter variation with plane direction can be seen. Finally, a comparison is done between experimental fatigue data obtained from the literature and estimated fatigue data. Lastly, it is proposed an alternative way of obtaining SSF damage map without relying on a paid software. The results obtained using the alternative approach is compared with the one obtained using Datafit.

In chapter 4 conclusions and future works are presented. This chapter starts with drawing the most relevant conclusions based on the SSF approach study that was done in chapter 3. In this chapter, it is also presented future developments that need to be addressed in order to better understand the SSF approach and also to validate the proposed methodology.

2. Literature review

2.1 Brief History of Fatigue

The term fatigue is derived from the Latin word *fatigo* which means get tired. The idea is that material gets tired just as humans do. So, when the material gets weakened and it is not replaced it will eventually fracture/fail. Fatigue is defined by ASTM [9] as "the process of progressive localized permanent structural change occurring in a material subjected to conditions which produce fluctuating stresses and strains at some point or points and which may culminate in cracks or complete fracture after a sufficient number of fluctuations".

As consequence of the industrial revolution, there was a rapid spread of railways that was initiated by Britain which then moved to other European countries, to America and finally it reached the world [10]. The development of faster trains allowed metal components to work under high stresses for the first time. The axles in the trains, for instance, were subjected to high cyclic loads. At this time not much was understood about the effect of high cyclic loads. A few years after the spread of railways across Europe, the first accident occurred near Versailles with an estimated 60 to 100 or more deaths was reported [11].

Due to the tragic accident near Versailles many engineers started considering fatigue failure in the design phase. For instance, August Wohler [12] carried out an experiment using miniature axle-like specimens, in order to understand the causes of Versailles accidents. The results obtained from the experiment demonstrated that a component may not fail when subjected to a particular load once whereas if that same amount of load is applied cyclically a complete fracture will occur. In addition to that the SN approach for fatigue life was established and the influence of areas of stress concentration in fatigue was introduced.

A key advance in understanding fatigue as a material problem were made in the beginning of 20th century. In 1903 Ewing and Humfrey [13] carried out an experiment using microscope to understand fatigue failure and also to determine the fatigue limit. The results of this microscopic study led to conclude that fatigue crack nuclei in a material start as micro cracks along slip-bands.

In 1910 an exponential power law that is based on the Wohler S-N approach was proposed by Basquin [14] . The proposed power law was based on the relationship between numbers of cycles required to cause failure and the stress used in endurance experiments. During the first 50 years of the 20th century the vast majority of studies considered stress-based

models, and this means that plastic deformation was not considered in the models at that time. Throughout the second half of 20th century there were many advances in the in nuclear power plant and aerospace industry, since plastic strain were dominant in the nuclear power plants, strain-based models began to gain more attention. In order to take into consideration, the plastic deformation Tavernelli and Coffin [15] and Manson [15] came up with a power law formula that can be related to the plastic strain with fatigue life.

In many engineering applications, components experience variable changing amplitudes rather than constant and they are also subjected to multiaxial loading not uniaxial loading. The first multiaxial studies were conducted by Lame and Tresca in their classical yield approach during the late 19th century and by von Mises in the beginning of 20th century.[16]. But these models were limited to in-phase loading condition only, for out of phase loadings these models would lead to ambiguous predictions.

For multiaxial loading condition several critical planes models were developed to account for both in-phase and out-of-phase loading. Studies about critical plane models that consider planes with maximum damage have been conducted over the last 50 years [17]. The critical plane approach can be applied both to proportional and nonproportional loading. The critical plane models are grouped as stress-based models (for high cycle fatigue), strain-based models (for high and low cycle fatigue) and energy-based models.

With regard to cycle counting methods to account for changes in amplitude several cycle counting techniques were developed in 1960s, with the rainflow being the most used. When it comes to quantifying the total damage that a component suffers, a cumulative damage developed by Palmgren-Miner is still widely used today.

With the introduction of many reliable numerical finite element software and with the development of many theories to account for variable amplitude changes as well as out-of-phase loading condition, the fatigue analysis became much more complete. However, it is worth mentioning that out of the many multiaxial models that exist not one of them account for all the factors that are involved in fatigue failures.

Despite significant advances in this field, many failures due to fatigue still take place. This means that more research is needed in order to improve the most used models or even to come up with the new ones.

2.2 Phenomenological fatigue behavior

In fracture mechanics theory, it is known that there is a certain condition in which a crack in a material is considered to be stable. This means that the material can safely operate at that condition. Thus, knowing the condition in which the material can work safely help engineers to build components or systems which the applied load will not cause fracture to take place.

A material that is subjected to repeated tensions will suffer microstructure modifications, known as fatigue. These modifications are not visible to naked eyes and failure can take place at stress level smaller than the elastic limit.

Fatigue process usually takes place in four stages, and these are as follows:

1. Crack nucleation.
2. Short crack growth(propagation).
3. Long crack growth(propagation).
4. Fracture.

It is known that no material ever produced is perfect, material usually have some defects which acts as stress concentrator. These defects may be geometric discontinuities, porosity inclusions. In Figure 2.1 a graphical representation of how fatigue process occurs is shown. It can be seen that crack nucleation starts in the areas of high stress concentration which is in the persistent slip bands. With the loading and unloading of the material, next step in the fatigue process starts to take place, this is the crack growth. Figure 2.1 shows that the second steps in fatigue process is divided in two stages. Stage I, crack nucleation and growth are usually considered to be the initial short crack propagation across a finite length of order of a couple of grains on the local maximum shear stress plane. In this stage, grain size, slip characteristics, orientation as well as stress level have great impact on the crack tip plasticity, this happens because material microstructure has a similar size to the crack tip. In stage II, when the material is cyclically loaded and unloaded, crack will start propagating and until it reaches a certain level it will move perpendicular to the applied load. Different from stage I, in this stage the characteristics of long crack growth suffer less influence from the microstructure characteristics, this is due to crack tip size being greater than the material microstructure [18].

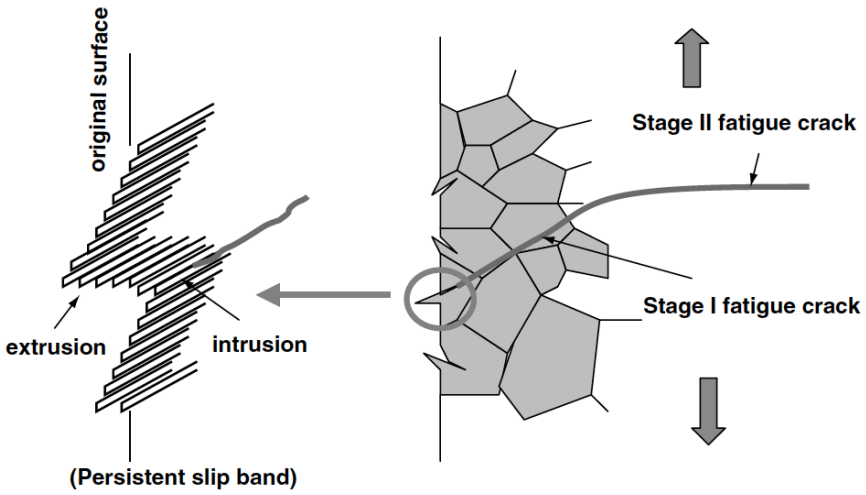

Figure 2.1 - Fatigue process of a thin plate under tensile loading [18].

In fatigue process, it is very important to differentiate crack nucleation stage to crack growth. This is because there are certain surface conditions such as roughness that affect the nucleation stage that can be negligible in the growth period. Corrosive environment is also a factor that affects nucleation phase differently to the growth phase [19].

2.3 Cycle loading description.

Each cycle in an alternating loading condition, as shown in Figure 2.2, is made of maximum stress, σ_{max}, minimum stress, σ_{min}, stress range $\Delta\sigma$, mean stress, σ_m stress amplitude, σ_a stress ratio R, and amplitude ratio A.

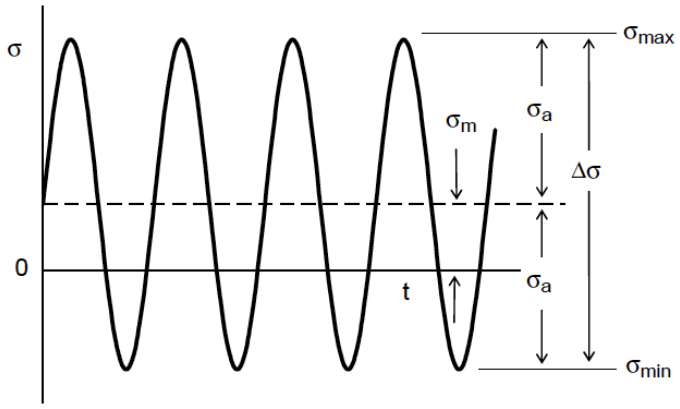

Figure 2.2 Typical cyclic loading with a constant amplitude [20].

From Figure 2.2 the following equations, Eq. (2.1) to (2.5), can be obtained:

$$\Delta\sigma = \sigma_{max} - \sigma_{min} \tag{2.1}$$

$$\sigma_a = \frac{\Delta\sigma}{2} \tag{2.2}$$

$$\sigma_m = \frac{\sigma_{max} + \sigma_{min}}{2} \tag{2.3}$$

$$R = \frac{\sigma_{min}}{\sigma_{max}} \tag{2.4}$$

$$A = \frac{1 - R}{1 + R} \tag{2.5}$$

When $R = -1$ means that there is a fully reversed condition, because $\sigma_{min} = -\sigma_{max}$ and for $R = 0$ when $\sigma_{min} = 0$ there is a pulsating tension. Most of fatigue data are obtained with zero mean stress, but it is important to mention that most of the engineering application such as automobile will require non-zero mean stress which means that it may be needed to apply some mean corrections [20].

2.4 Critical plane models

The basis of using critical plane models came from experimental observations of cracks nucleation and growth during loading. Factors such as stress state, type of material and strain amplitude will determine if fatigue life will be dominated by crack growth along tensile or shear planes.

Critical plane models are grouped in three categories: stress based, strain based, and energy based. A strain-based model is suitable for applications that involves a low cycle fatigue whereas stress-based model is for high cycle fatigue applications. Energy based models [22] is made of three groups depending on their application: for high cycle fatigue, the criteria based on elastic strain energy is appropriate, for low cycle criteria based on elastic stress energy is suitable and for applications which both low and high cycle are present, the criteria based so the sum of elastic strain and stress energy is used.

The critical plane approach is used not only to determine the fatigue life of a component but also to identify their failure plane(s). In the critical plane approach, the plane that experiences the highest damage is the critical plane. Critical plane approaches are well accepted for multiaxial loading condition. For a critical plane model to be considered as a good model, it should be able to predict fatigue life reasonably and also the dominant failure plane.

2.4.1 Local and global stresses

The damage parameter in the stress based critical plane models is determined on local stress in each orientation (plane). This is based on the Mohr circle, which is graphical methodology that allows to do state stress transformations. By doing this, the aim of the critical plane model basically is to find which orientation the damage parameter has a maximum value. In order to identify which plane experience the highest damage equations (2.6) and (2.7) are used. As shown in Figure 2.3 these equations are based on global and normal stress components.

$$\sigma_{\theta,local}(t) = \frac{\sigma_{x,global}(t) + \sigma_{y,global}(t)}{2} + \frac{\sigma_{x,global}(t) - \sigma_{y,global}(t)}{2}\cos(2\theta) + \tau_{xy,global}\sin(2\theta) \tag{2.6}$$

$$\tau_{xy,local}(t) = \frac{\sigma_{x,global}(t) - \sigma_{y,global}(t)}{2}\sin(2\theta) - \tau_{xy,global}\cos(2\theta) \tag{2.7}$$

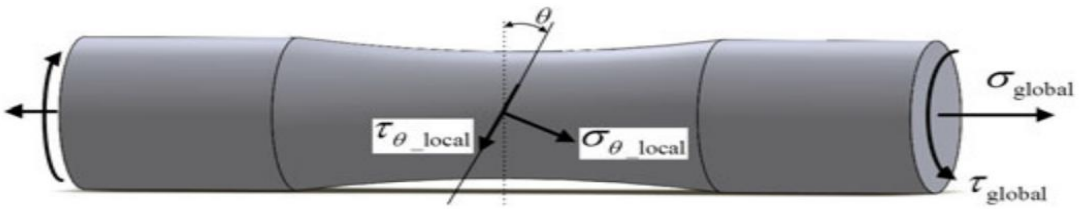

Figure 2.3 Shows the global and local stresses on a sample[23].

2.4.2 Brown-Miller

Brown and Miller [24] conducted a tension-torsion experiment with a constant shear strain of 0.03. The data collected from their experiment can be seen in Figure 2.4. The conclusion that was drawn from their test is that two strain parameters should consider when describing a fatigue process. These parameters are cyclic shear and normal strain that is acting on the plane of maximum shear.

Brown and Miller [25] proposed a multiaxial fatigue approach which is based on observations of fatigue crack growth processes and thus has a physical interpretation. The

fatigue failure in this approach is expressed by a non-linear equation made of strain parameters as shown in Eq. (2.8).

$$\frac{\varepsilon_1 - \varepsilon_3}{2} = f\left[\frac{\varepsilon_1 + \varepsilon_3}{2}\right] \tag{2.8}$$

Where $\varepsilon_1, \varepsilon_2, \varepsilon_3$ are principal strains, $\varepsilon_1 \geq \varepsilon_2 \geq \varepsilon_3$.

$$\varepsilon_n = \frac{\varepsilon_1 + \varepsilon_3}{2} \tag{2.9}$$

$$\frac{\gamma}{2} = \frac{\varepsilon_1 - \varepsilon_3}{2} \tag{2.10}$$

The plane that has the highest shear strain value is the critical plane. However, this non-linear equation only holds true for a proportional loading condition in which the principal strain terms are assumed to be fixed.

Brown and Miller realized that it is possible to have the same shear strain with two different loading cases. Because of that Brown and Miller considered two types of cracks that are illustrated in Figure 2.4. From Figure 2.4 Case A, it can be observed that in this situation the crack growth takes place along the material surface and this is what happens in torsional loading condition. For a case B crack, which is a biaxial tension case, the shear stress drives the crack propagation through the material thickness away from the surface. A crack B type intersects the surface at an angle of 45 degrees. For a tension loading condition, both case A and case B would have the same shear stress and can demonstrate both modes of cracking. However, for a biaxial loading condition (tension-torsion) a case A crack is always displayed.

Both crack A and crack B are expressed using Eq. (2.11) and (2.12).

Case A: $$\left(\frac{\Delta\gamma}{g}\right)^j + \left(\frac{\varepsilon_n}{h}\right)^j = 1 \tag{2.11}$$

Case B: $$\frac{\Delta\gamma}{2} = constant \tag{2.12}$$

Where: $\frac{\Delta\gamma_{max}}{2}$ is the maximum shear strain amplitude, $\Delta\varepsilon_n$ is the normal strain that acts on the plane of maximum shear, S is the normal strain coefficient.

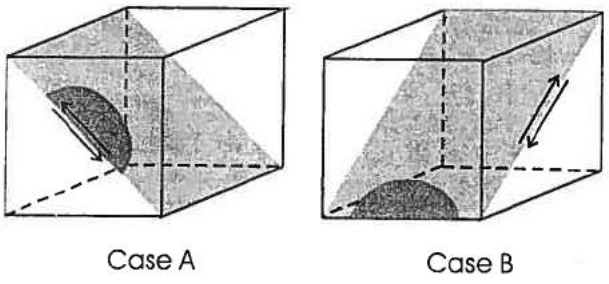

Figure 2.4 Case A and Case B cracks [24].

The values of g and h have to be determined and the value of j varies from 1 for brittle material and 2 for ductile materials. Later on, Kandil, Miller and Brown [49] proposed a simplified expression, see Eq. (2.13), for crack A type and this also includes the effect of mean stress.

$$\frac{\Delta\gamma_{max}}{2} + S\Delta\varepsilon_n = (1.3 + 0.7S)\frac{\acute{\sigma_f} - 2\sigma_{n,med}}{E}\left(2N_f\right)^b + (1.5 + 0.5S)\acute{\varepsilon_f}\left(2N_f\right)^c \tag{2.13}$$

From the above equation, the mean stress influences are included using Morrow´s mean stress approach from on the right side of the equation.

The S value will vary from one material to another, and they can be determined through tension and torsional experiments. Figure 2.5 shows how the S value changes as the number of cycles increases.

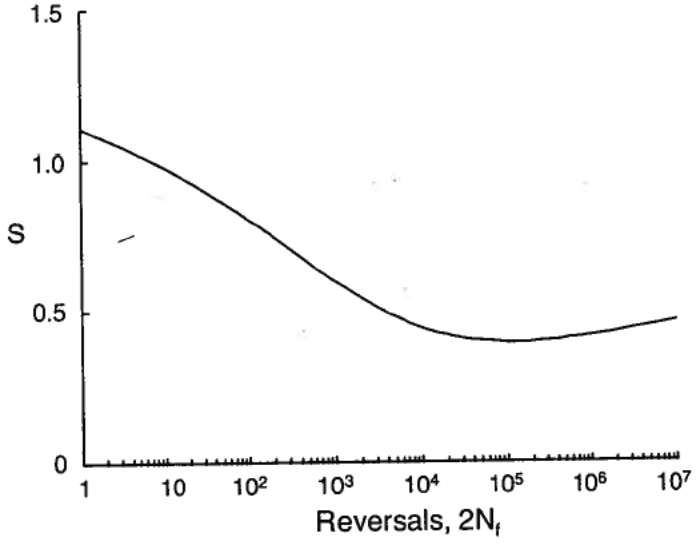

Figure 1.5 Variation of normal strain coefficient with number of cycles [24].

The critical plane can be estimated using the Eq. (2.14), and it will be the plane in which the shear strain reaches maximum value.

$$\left(\frac{\Delta\gamma_{max}}{2} + S\Delta\varepsilon_n\right)_{max} \tag{2.14}$$

2.4.3 Fatemi-Socie

Fatemi-Socie developed a critical plane approach that is based on Brown-Miller's work. Since the Brown-Miller approach is represented in terms of strain and it does not consider the effect of cyclic hardening, many authors have considered these to be the reason that the out-of-phase loading cause more damage than the in-phase loading [26], [27]. To take into account the effect of cyclic hardening that is caused by the rotation of the principal axes in nonproportional loading condition Fatemi-Socie proposed a modification to Brown-Miller approach, the strain term was changed with a normal stress [28]. Figure 2.6 illustrates the physical significance of this model.

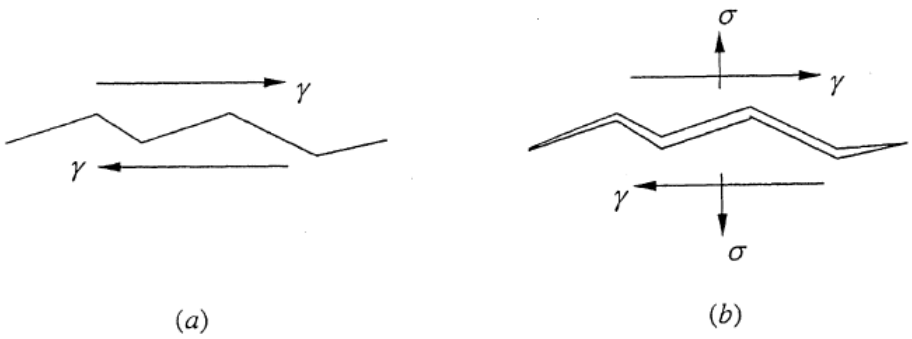

Figure 2.6 Illustration of the physical significance of Fatemi-Socie model:(a) shear loading of a crack, (b) effect of tensile stress on the shear crack [29].

From Eq. (2.15) it can be seen that the governing parameters in the Fatemi-Socie approach are Maximum shear strain amplitude and maximum normal stress that is acting on the maximum shear plane amplitude. It is known that typically crack have a nonuniform shape this means that during shear loading the increase in crack will result in frictional forces between crack surfaces, the frictional forces will hinder the crack growth which will finally lead to a longer fatigue life (Figure 2.6a). From Figure 2.6b it can be seen that the applied tensile stress will separate both crack surfaces which will result in reduction and frictional forces as well as fatigue life.

$$\frac{\Delta\gamma_{max}}{2}\left(1 + k\frac{\sigma_{n,max}}{\sigma_y}\right) \tag{2.15}$$

Socie and Shield [30] carried several biaxial experiments using Inconel 718 specimens so that the impact of maximum normal stress could be assessed. The test was conducted at room temperature with the specimens subjected to both tension-torsion strain control. The results obtained from these tests showed that material that experience Mode II type of failure will always be the maximum shear strain amplitude plane. From the experiment it was also concluded that the fatigue life, the preferred maximum shear plane as well as crack distribution are influenced by the mean stress value, but the mean stress does not influence in which direction crack goes or in which mode the material will fail.

The Fatemi-Socie critical plane approach is ideal for material that fail under mode II. Different from Brown-Miller approach, this approach can be used to examine the influence of mean stress and the effect of nonproportional hardening. In relation to fatigue life, the Fatemi-Socie approach can be expressed using Eq.(2.16):

$$\frac{\Delta\gamma_{max}}{2}\left(1 + k\frac{\sigma_{n,max}}{\sigma_y}\right) = \frac{\tau'_f}{G}\left(2N_f\right)^{b_\gamma} + \gamma'_f\left(2N_f\right)^{c_\gamma} \tag{2.16}$$

Where: $\frac{\Delta\gamma_{max}}{2}$ is the maximum shear strain amplitude, $\sigma_{n,max}$ is the maximum normal stress acting on the maximum shear plane amplitude, σ_y is the yield stress, k is the material constant that is obtained through test, τ'_f is the shear fatigue strength coefficient, G is the shear modulus, N_f is number of cycles to failure, γ'_f is the shear fatigue ductility coefficient and finally b_γ, c_γ are shear fatigue strength exponent and shear fatigue ductility exponent. These parameters and exponents can be determined through tension and torsion tests. From Figure 2.7, the variation of K coefficient with the number of cycles is shown, so based on this figure the K parameter can be estimated if the number of cycles is known.

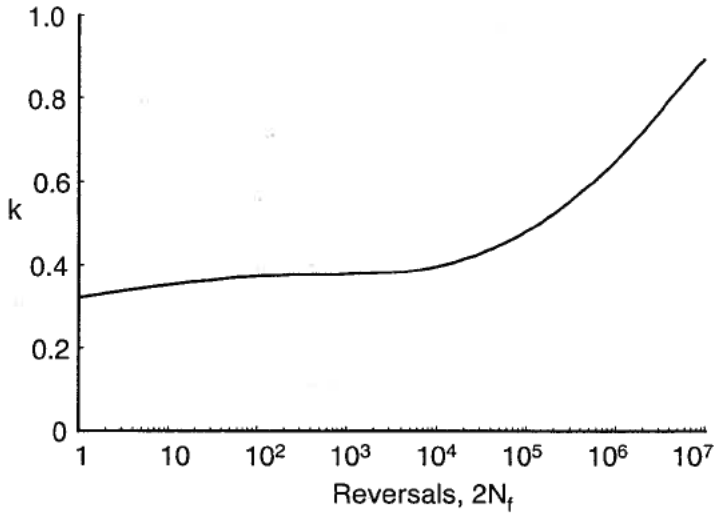

Figure 2.7 Variation of K coefficient with number of cycles [24].

For out-of-phase multiaxial loading, the critical plane can be determined using the Eq. (2.17). Critical plane will be the plane in which the constant value is maximum.

$$\left[\frac{\Delta\gamma_{max}}{2}\left(1+k\frac{\sigma_{n,max}}{\sigma_y}\right)\right]_{max} \tag{2.17}$$

2.4.4 Smith, Watson and Topper (SWT)

In 1970 Smith, Watson and Topper [31] proposed a model that can be applied to both proportional and nonproportional loading condition. The approach was developed to consider materials that fail under maximum tensile stress or strain.

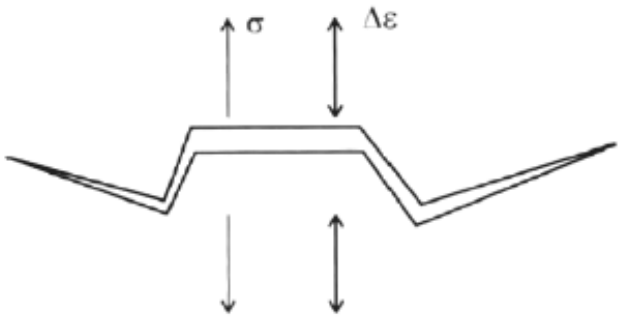

Figure 2.8 Physics behind SWT parameter [24].

In the case of uniaxial loading, this model is used as tool to take into account the effect of mean stress. For multiaxial loading condition, the SWT model combines both maximum stress and principal strain range as the governing parameter. As can be observed from Figure 2.8, in the situation which microcrack grows in mode I, the driving force would be the stress that is opening those microcrack in the principal strain plane. The expressions that describe the SWT parameter can be obtained by manipulating the Morrow's expressions, see Eq. (2.18) to (2.21).

$$\varepsilon_a = \frac{\acute{\sigma_f}}{E}\left(2N_f\right)^b + \acute{\varepsilon_f}\left(2N_f\right)^c \tag{2.18}$$

$$\sigma_a = \acute{\sigma_f}\left(2N_f\right)^b \tag{2.19}$$

$$\sigma_{max}\varepsilon_a = \acute{\sigma_f}\left(2N_f\right)^b\left[\frac{\acute{\sigma_f}}{E}\left(2N_f\right)^b + \acute{\varepsilon_f}\left(2N_f\right)^c\right] \tag{2.20}$$

$$\sigma_{max}\frac{\Delta\varepsilon_1}{2} = \frac{\acute{\sigma_f^2}}{E}\left(2N_f\right)^{2b} + \acute{\sigma_f}\acute{\varepsilon_f}\left(2N_f\right)^{b+c} \tag{2.21}$$

Where: σ_{max} is the maximum tensile stress on the plane of principal strain, ε_a is the maximum strain amplitude, $\acute{\sigma_f}$ is the axial fatigue strength coefficient, E is the Young's modulus, N_f is the number of cycles to failure, $\acute{\varepsilon_f}$ is the axial fatigue ductility coefficient and finally b, c are axial fatigue strength exponent and axial fatigue ductility exponent respectively.

The stress term used in this model makes it suitable for describing mean stresses during multiaxial loading and nonproportional loading effects [24]. Concerning the critical plane, the SWT parameter is calculated from the plane in which the principal strain range is highest, and this is done using Eq. (2.22).

$$\left(\sigma_{max}\frac{\Delta\varepsilon_1}{2}\right)_{max} \tag{2.22}$$

2.4.5 Liu

A model based on virtual strain energy (VSE) was proposed by Liu [32]. This model different from others, it takes into consideration both mode I (opening) and mode II (shearing) failure. For each plane, the virtual strain energy is made of plastic and elastic work, see Eq. (2.23). From Figure 2.9, the elastic work is represented by the shaded area which can be determined by adding both of these areas and the plastic work can be determined by multiplying $\Delta\sigma.\Delta\varepsilon_p$.

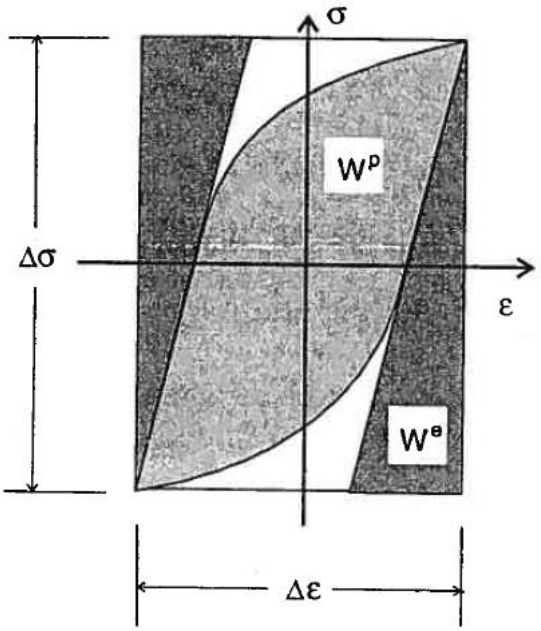

Figure 2.9 Representation of elastic and plastic strain energy [24].

$$\Delta W = \Delta W^e + \Delta W^p \cong \Delta\sigma \cdot \Delta\varepsilon \tag{2.23}$$

Using the strain-life equations, ΔW is determined using Eq. (2.24).

$$\Delta W = 4\acute{\sigma}_f \acute{\varepsilon}_f \left(2N_f\right)^{b+c} + \frac{4\acute{\sigma}_f^2}{E}\left(2N_f\right)^{2b} \tag{2.24}$$

The virtual strain energy method in a multiaxial loading case considers failure due to tensile, ΔW_I, and failure caused by shear, ΔW_{II}. For a shear failure, as in the Brown-Miller approach, the VSE considers both type A and type B cracks. The VSE parameter for a tension-torsion loading is given by Eq. (2.25).

$$\Delta W = \Delta W_I + \Delta W_{II} \tag{2.25}$$

The fact that the work quantities are defined for specific plane within the material made the Liu model to be considered as a critical plane model [24]. Failure in this model is expected to take place in the plane that has the highest VSE quantity. On the one hand, the axial work, ΔW_I is calculated by multiplying the ranges of normal strain and stress on the plane of its maximum value and then is added by how much shear is there, see Eq. (2.26).

$$\Delta W_I = (\Delta\sigma\Delta\varepsilon)_{max} + (\Delta\tau\Delta\gamma) \tag{2.26}$$

To determine fatigue life, Eq. (2.27) is used.

$$\Delta W_I = 4\acute{\sigma_f}\acute{\varepsilon_f}\left(2N_f\right)^{b+c} + \frac{4\acute{\sigma_f^2}}{E}\left(2N_f\right)^{2b} \tag{2.27}$$

Just as ΔW_I, the shear work ΔW_{II} is estimated by the product of ranges of normal shear stress and shear strain on the plane of its maximum value and then is added with the axial work on that same plane, see Eq. (2.28).

$$\Delta W_{II} = (\Delta\sigma\Delta\varepsilon) + (\Delta\tau\Delta\gamma)_{max} \tag{2.28}$$

For fatigue life estimation Eq. (2.29) is used.

$$\Delta W_{II} = 4\acute{\tau_f}\acute{\gamma_f}\left(2N_f\right)^{b_\gamma+c_\gamma} + \frac{4\acute{\tau_f^2}}{G}\left(2N_f\right)^{2b_\gamma} \tag{2.29}$$

Where: $\Delta\tau$ and $\Delta\gamma$ are normal shear stress and shear strain, $\Delta\sigma$ and $\Delta\varepsilon$ are the normal stress and normal strain, G is the shear modulus, $\acute{\tau_f}$ is the shear fatigue strength coefficient, G is the shear modulus, N_f is number of cycles to failure, $\acute{\gamma_f}$ is the shear fatigue ductility coefficient, b_γ and c_γ are shear fatigue strength exponent and shear fatigue ductility exponent.

For a tensile failure mode there is only one critical plane, whereas for a shear failure mode there are two critical planes for each type of crack that are separated at 90 degrees. For uniaxial loading condition $\Delta W_{II,A} = \Delta W_{II,B}$. However, for a tension or combination of both tension and torsion $\Delta W_{II,A} > \Delta W_{II,B}$. $\Delta W_{II,B}$ will be predominant in the case of tension-compression loading. Amongst the three parameters, $\Delta W_I, \Delta W_{II,A}, \Delta W_{II,B}$ which one is going to dominate will depend on the type of loading, on the material used as well as on the temperature.

2.5 Normal and shear stress scale factor

Most multiaxial models evaluate the overall damage by combining the damaged caused by shear and normal stress. Typically, in multiaxial fatigue models, a combined axial and shear damage effect on the fatigue process is described by the stress scale factor.

The concept of stress scale was used for the first time by von Mises criterion, a factor of $\sqrt{3}$ was used to transform the shear stress into normal stress scale, see Eq. (2.30). One other example which uses this concept is the Tresca yield criterion, in this case a factor of $\frac{1}{2}$ is used to update the principal stresses to the shear stress scale, see Eq. (2.31).

$$\sqrt{3}\tau = \sigma \tag{2.30}$$

$$\tau_{tresca} = \frac{\sigma_1 - \sigma_3}{2} \tag{2.31}$$

Both von Mises and Tresca criterion consider a constant scale regardless of the type loading condition. However, the SSF approach takes into account the type of loading and its stress intensity.

2.6 SSF equivalent shear stress

The SSF is damage scale that relates axial and shear stresses, it was develop by the following authors [33]. The SSF approach is based on the damage scale relationship between damage caused by both axial and shear components.

Reis et al [34], [35] conducted several studies using the low alloy steel 42CrMo4, the findings from this studies showed that stress intensity level as well the loading path will have an effect on the damage scale between normal and shear components. Because of that, instead of considering a constant stress scale, the SSF approach uses variable stress scale to determine normal and shear damage.

In order to have the same damage scale, the SSF criterion allows a normal stress to be added with shear stress by transforming the normal stress component into shear damage scale, this is done using Eq. (2.32).

$$\mathrm{T}(\tau, \sigma) = \tau + \mathrm{SSF}(\sigma, \lambda)\sigma \tag{2.32}$$

Where: σ and τ are the instantaneous normal and shear stresses and SSF is the polynomial function of 5th order which converts the fatigue damage of normal stresses into shear damage scale and it can be determined using Eq. (2.33).

$$\mathrm{SSF}(\sigma,\lambda) = \mathrm{a} + \mathrm{b}.\sigma + \mathrm{c}.\sigma^2 + \mathrm{d}.\sigma^3 + \mathrm{f}.\lambda^2 + \mathrm{g}.\lambda^3 + \mathrm{h}.\lambda^4 + \mathrm{i}.\lambda^5 \qquad (2.33)$$

where: $\mathrm{a} = 2.69$; $\mathrm{b} = -9.90\mathrm{E}-03$; $\mathrm{c} = 1.69\mathrm{E}-05$; $\mathrm{d} = -9.52\mathrm{E}-09$;
$\mathrm{f} = -5.99$; $\mathrm{g} = 11.72$; $\mathrm{h} = -8.04$; $\mathrm{i} = 1.63$

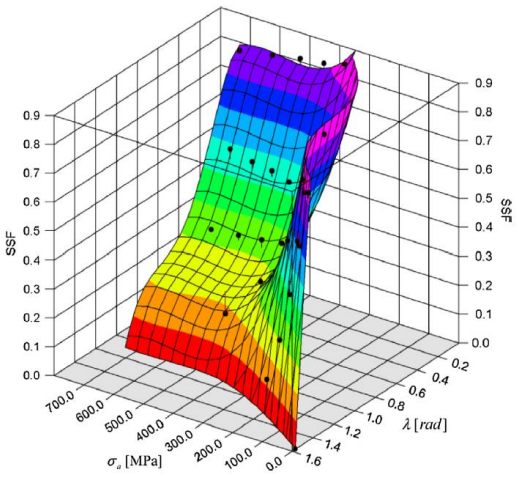

Figure 2.10 SSF surface for 42CrMo4 at 0°.

σ is the instantaneous value of the normal stress of a biaxial loading and $\lambda = \frac{\tau}{\sigma}$ is the instantaneous stress amplitude ratio. All the constants in the equation 2.33 can be determined by experiments.

With regard to fatigue life, it is estimated under constant amplitude loading using the maximum SSF equivalent shear stress, see Eq. (2.34).

$$\left(\tau_{eq}\right)_{max,block} = \max_{block}(\tau + SSF(\sigma,\lambda)\sigma) = A\left(N_f\right)^b \qquad (2.34)$$

where: σ and τ are the instantaneous load components, A and b are parameters of the uniaxial SN shear curve of a given material, N_f is the fatigue strength subjected to certain stress level and $SSF(\sigma,\lambda)$ is stress scale factor that is determined using equation 2.33.

In order to estimate fatigue life, a uniaxial SN curve, see Eq. (2.35), under pure shear was determined through experimental results.

$$\tau = 864.78\left(N_f\right)^{-0.061} \tag{2.35}$$

To allow the use of SSF damage map that was developed using 42CrMo4 to be used for other materials from the same family the authors presented an expression, see Eq. 2.36, that can be used to update the SSF damage map using material ultimate tensile stress [36].

$$\tau_{eq} = \tau + \left(\frac{\sigma_u}{\sigma_{u,42CrMo4}}\right) SSF(\sigma, \lambda)\sigma \tag{2.36}$$

Where: $\frac{\sigma_u}{\sigma_{u,42CrMo4}}$ is the ratio between the material's ultimate tensile stress (material must be part of the 42CrMo4 family with an unknown SSF damage map) and the ultimate tensile stress of the 42CrMo4 steel.

2.7 Uniaxial cycle counting

In order to estimate fatigue life of a component it is necessary to know the number of cycles that can operate before failure. So, engineers use small specimen in laboratory experiments to understand material behaviour in tension, compression or torsion. When the material is loaded and unloaded this information is collected and plotted in stress and strain graph to see how the material reacts when load is applied.

The number of cycles is counted from the process of loading and unloading. Components may experience tension, bending or torsion simultaneously generating cycles which cannot be easily counted. For instance, when an airplane is flying it generates very complex and complicated loading history, which makes very hard the task of knowing where one cycle starts and finishes.

The American Society for Testing Materials [37] defines a cycle under constant amplitude as "the load variation from the minimum to the maximum and then to the minimum load". Regarding the loading history, a cycle is represented by closed-loop stress-strain hysteresis loop. The purpose of using cycle counting techniques is to convert a complex loading history into simpler one that has relationship with fatigue damage.

In this section two approaches of cycle counting will be discussed, one-parameter and two parameters. Firstly, one-parameter cycle counting such as level crossing, peak-valley and range cycle counting will be discussed, and their strengths and limitation highlighted. And then the two-parameters methods will also be discussed. Finally, two variants of the Rainflow algorithm namely three and four points methods will be look at.

2.7.1 One-Parameter cycle counting

- **2.7.1.1 Level-crossing cycle counting**

The process of counting in this method is performed by first diving the applied loads into various levels that have equal increment as can be seen from Figure 2.11. To do the counting a reference value of stress is selected and then from there the counting is recorded as the positive sloped portion of the stress crosses the reference value. Similarly, a cycle is counted as the negative sloped portion of the stress crosses the reference value below the reference value.

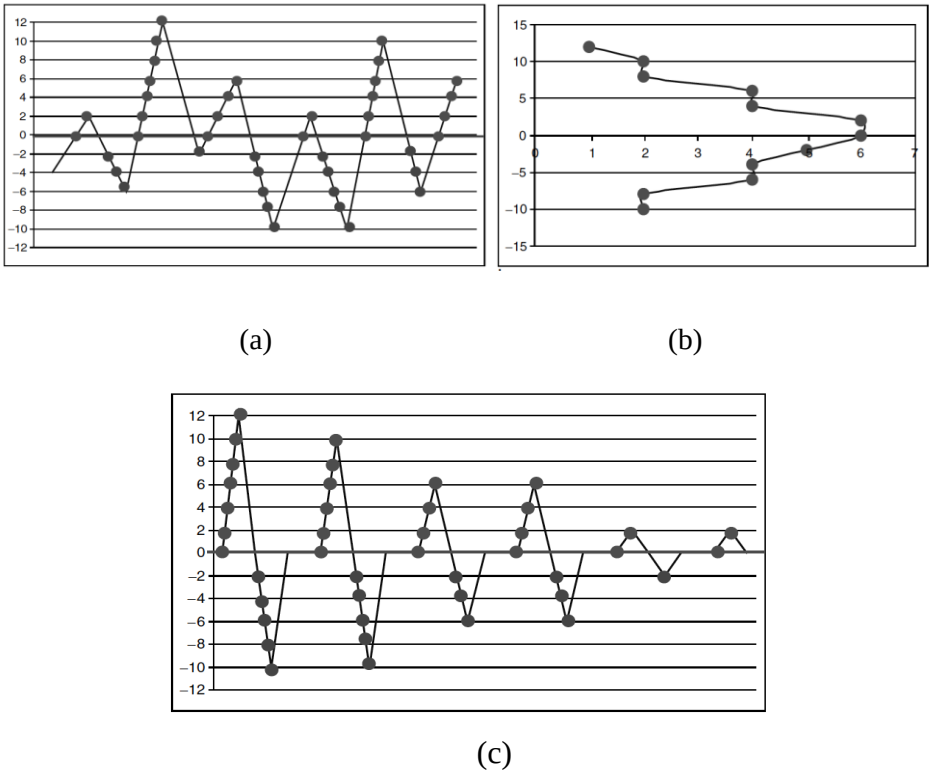

Figure 2.11 (a) Load-time history in level crossing counting , (b) level crossing counting plot and(c) Cycle generation in level crossing counting [18].

- **2.7.1.2 Peak-valley cycle counting**

In this method, the cycle counting is performed by considering the maximum and minimum value of the load previously identified from the loading history. Based on these values the possible cycles are formed starting from the event with the most damage to the event with least damage, this is all done according to the peak-valleys that were extracted.

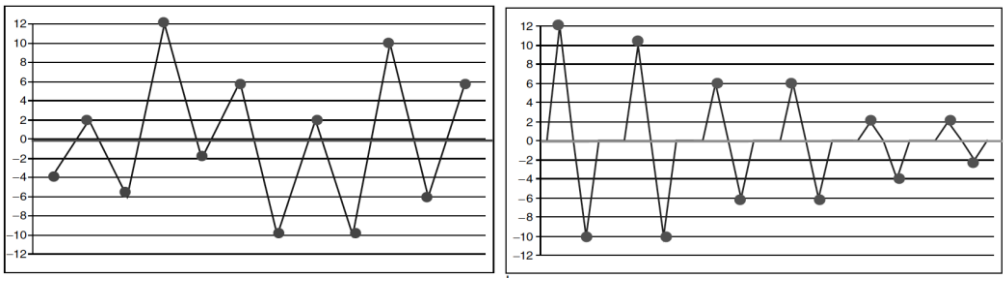

(a) (b)

Figure 2.12 Load-time history in Peak-Valley cycle counting and (b) Process of generating cycles [18].

- **2.7.1.3 Range cycle counting**

In this method each counting is defined as range. The range is obtained by subtracting two successive reversals. The range will be positive or negative depending on whether the valley follows the peak, or a peak is followed by a valley. This method is also called simple range-mean if the mean value of each range is counted [37].

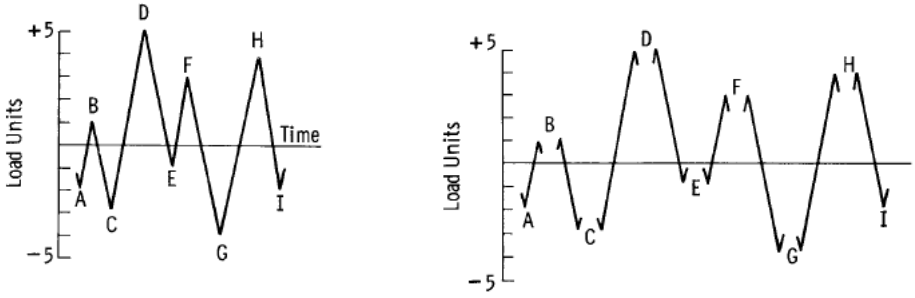

(a) (b)

Figure 2.13 (a) Peaks and Valleys identified and (b) cycle generation in range counting[37].

For many years, due to their simplicity the one parameter techniques were frequently used to extract cycles from complex history. But all one parameter cycle counting methods are not very practical in terms of quantifying fatigue damage, and this is because it does not give

a very practical description of a cycle. In addition to that all one-parameters methods do not properly link the closed loop stress and strain hysteresis to the loading cycle which is known to have a great effect on fatigue failure [18]. Therefore, even though all one-parameter are easy to apply, these cycle counting techniques are considered improper to analyse fatigue damage.

2.7.2 Two-parameter cycle counting

In order to overcome the limitations of all one parameter methods, which fails to link loading cycle to hysteresis closed loop, two parameter counting techniques named “Rainflow” were developed in 1968 by Japanese professor Matsuishi and Endo [38]. The concept behind the rainflow method comes “to the flow of rain failing on a pagoda and running down the edges of the roof**.** The cycle counting process of the Rainflow method is illustrated by figures 2.14 and 2.15 and it is applied using the following rules:

- Starting from a maximum (minimum) peak, the rainflow will stop when a maximum (minimum) peak which is larger (smaller) than the peak appears.

- If a rainflow meets the raindrop fallen from an upper roof the rainflow stops at that place.

Figure 2.14 Load-time history [39].

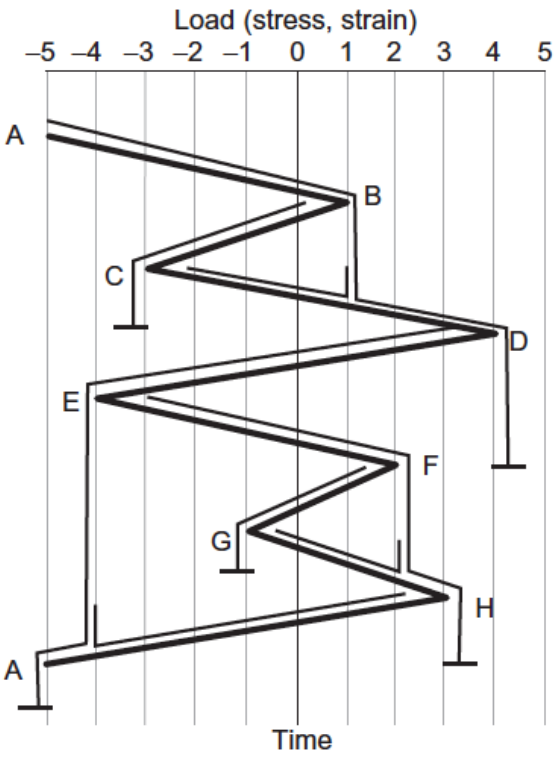

Figure 2.15 Application of the rainflow method to load-time history [39].

In order to apply the rainflow methods in a practical applications Downing and Socie [40] developed two algorithms to do the cycle counting. Among the two algorithms the one-pass rainflow is widely used in engineering application. One-pass rainflow is used instead of the other algorithm because it overcomes the main problem associated with another algorithm. The main problem in using other algorithm is that cycles can only be counted if the whole loading history is known prior to the counting process. There are many cycles counting techniques that are based on the rainflow method, but in this section only two will be discussed: three-point [41] and four-point algorithm[42].

- **2.7.2.1 Three-point method**

The cycle counting process in the three points technique is done using three consecutive points. These three points will show if a cycle is generated or not.

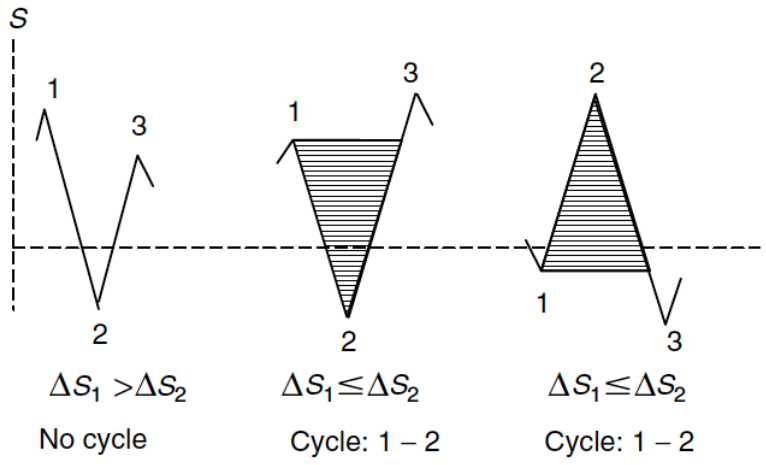

Figure 2.16 Steps to perform cycle counting [18].

The consecutive points from Figure 2.16 are S_1, S_2, and S_3, with these points two consecutives ranges can be calculated using the Eq. (2.37) and (2.38)

$$\Delta S_1 = |S_1 - S_2| \tag{2.37}$$

and

$$\Delta S_2 = |S_2 - S_3| \tag{2.38}$$

The formation of cycles depends on whether the point 1 has higher or lower value than point 2. Cycles are not created when the load value at point 1 is higher than at point 2. The cycle counting is done by first rearranging the load history, the rearrangement is done by maintaining only peaks and valleys. The rule is to begin with lowest valley or with highest peak. The two points that create a cycle are neglected and the remaining are connected to one another. This process is repeated until all the data become exhausted.

- **2.7.2.2 Four-point method**

In the same manner as the three points cycle counting, the way of extracting cycles is by selecting four consecutive points. In this case there are 4 consecutive points (S_1, S_2, S_3, and S_4,) in the load-time graph (see Figure 2.17). With these points the inner and outer ranges are defined by Eq. (2.39) and (2.40).

$$\Delta S_1 = |S_2 - S_3| \tag{2.39}$$

and

$$\Delta S_0 = |S_1 - S_4| \tag{2.40}$$

In the four-point approach there are: standing cycle and hanging cycle, which are two possible cycles of the loading history shown in Figure 2.17.

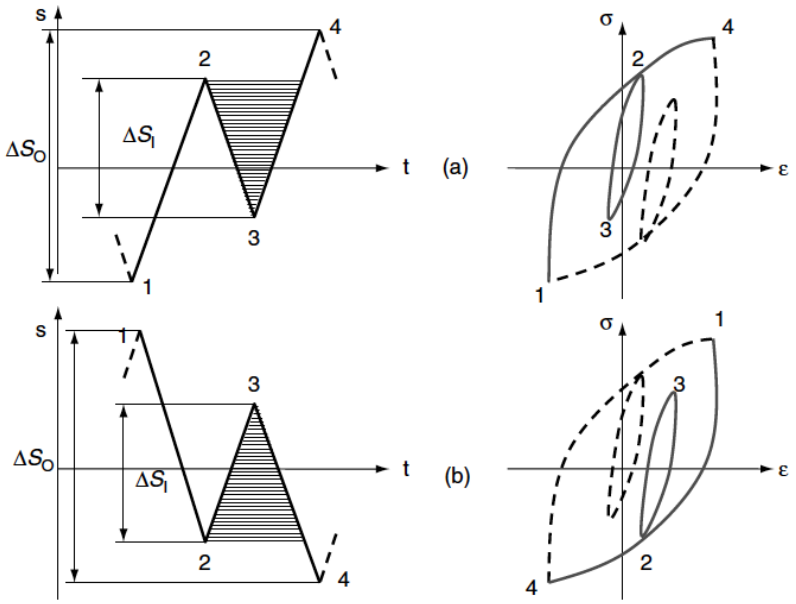

Figure 2.17 Cycle counting process in four-point rainflow method;(a) hanging cycle and (b) standing cycle [18].

Cycles are only counted from points S_2 to S_3, if $\Delta S_0 \gg \Delta S_1$ and also if the points of the inner range are enclosed by those of the outer range.

The difference between four points and three points is that in the four points method there is no assurance that all the points will end up forming a cycle and those points that do not form a cycle are named as residue.

It is also important to mention that the three points method can be obtained from the four points one. Mclnnes and Meehan [43] in their work concluded that both three points and four points technique are equivalent, this is because even changing the input stress series the four points algorithm the overall result was not affected. It was shown that even after these changes both three and four points algorithms were able to identify equal hysteresis loop and in equal order.

Even though rainflow methods remains the most used there are some drawbacks associated to it, they do not capable of accurately calculate cycles involving complex loadings conditions [44]. Another drawback pointed by Moshrefifar and Azamfar is that the Rainflow method sometimes ignores the maximum amplitude principles, for this reason it is not applicable to all situations [45]. Langlais [46] pointed data rainflow is only able to identify cycles through peaks and valleys.

Results coming from rainflow and range methods have very good agreement with experimental results and because of that these two methods are recognized as the best in uniaxial random loading [47].

2.8 Multiaxial cycle counting

Most engineering components namely turbines, crank shaft, pressure vessels and transmission systems experience multiaxial stress state with variable or random loading condition. In many cases the load that is applied may be proportional or non-proportional. Proportional loading means that the principal stresses directions are constant whereas in non-proportional loading those principal stresses change with time.

The understanding of multiaxial fatigue remains very complex problem to deal with, since the component or system is subjected to many strain or stress simultaneously. However, from 1970 until today many works are being done in multiaxial fatigue and new theories or improvement of the old ones are coming out. Even though, there are improvements in the multiaxial fatigue there is still a lack of agreement among the scientific community about which theories is the best [41]. In practical application because most components experience changes in magnitude as well as direction, the uniaxial loading should also be studied as non-proportional multiaxial loading [48].

In general service load histories are multiaxial and not uniaxial. The use of classical models such as von Mises in multiaxial loading case usually leads to poor results, this model work better for proportional loading cases. For multiaxial loading case, critical plane models which seeks for a plane that experiences the most damage, yields better results than the classical models, and this makes it more acceptable for multiaxial cases [49]. One great aspect of the critical plane approach is that when both stress and shear terms are included in its model they can used both in applications related to high cycle fatigue and also to low cycle fatigue and the critical plane approach are also able to capture material constitute response in non-proportional loading [16].

There are many challenges associated with predicting a fatigue life of a component under multiaxial loading. For instance, Wei and Dong [50] have pointed that there is still lack of proper definition of stress/strain damage parameter and also the cycle counting that are available today continue to demonstrates some inconsistencies. On the other hand, compared to uniaxial method the hysteresis is not properly defined in the multiaxial fatigue [46]. In this section some multiaxial cycle counting techniques will be described.

2.8.1 Wang and *Brown*

During the 90s, Wang and Brown [51] came up with new cycle counting method that can be applied to both proportional and non-proportional loading [49]. The WB method is based on the equivalent stress/strain approach. In order to do the cycle counting it uses the von Mises criterion together with the Rainflow cycle counting.

In this method the von Mises is used as an indirect measure of fatigue damage [52] . The application of von Mises criterion serves to convert a complex multiaxial state stress to uniaxial state. The von Mises equivalent strain can be expressed as:

$$\varepsilon_{eq} = \frac{1}{\sqrt{2}(1+\nu)}\sqrt{\left(\varepsilon_x - \varepsilon_y\right)^2 + \left(\varepsilon_y - \varepsilon_z\right)^2 + (\varepsilon_z - \varepsilon_x)^2 + \frac{3}{2}\left[\gamma_{xy}^2 + \gamma_{yz}^2 + \gamma_{xz}^2\right]} \qquad (2.41)$$

Where: ε_{eq} is the equivalent strain, ε_x, ε_y and ε_z are the strain components; γ_{xy} , γ_{yz} and γ_{xz} are the shear strain components and ν is the effective Poisson ratio (the average of the elastic and plastic coefficients, typically it is 0.5), and it is expressed by Eq. (2.42):

$$A\nu = \frac{\nu^e \varepsilon^e + \nu^p \varepsilon^p}{\varepsilon} \qquad (2.42)$$

The problem with the equivalent Von Mises strain is that it does not recognized fatigue process as directional. This means that the Von Mises value is always positive regardless of the direction of the applied load. Because of this shortcoming, fatigue life prediction may sometimes be wrongly predicted. Therefore, to overcome the sign shortcoming Wang and Brown used relative equivalent strain, which is calculated using the expression (2.43):

$$\varepsilon_{eq}^{rel} = \frac{\sqrt{\left(\Delta\varepsilon_x - \Delta\varepsilon_y\right)^2 + \left(\Delta\varepsilon_y - \Delta\varepsilon_z\right)^2 + (\Delta\varepsilon_z - \Delta\varepsilon_x)^2 + \frac{3}{2}\left[\Delta\gamma_{xy}^2 + \Delta\gamma_{yz}^2 + \Delta\gamma_{xz}^2\right]}}{\sqrt{2}(1+\nu)} \qquad (2.43)$$

where: $\Delta\varepsilon_x = \varepsilon_x(j) - \varepsilon_x(i)$, $\Delta\varepsilon_y = \varepsilon_y(j) - \varepsilon_y(i)$, $\Delta\varepsilon_z = \varepsilon_z(j) - \varepsilon_z(i)$, $\Delta\gamma_{xy} = \gamma_{xy}(j) - \gamma_{xy}(i)$, $\Delta\gamma_{xz} = \gamma_{xz}(j) - \gamma_{xz}(i)$, $\Delta\gamma_{yz} = \gamma_{yz}(j) - \gamma_{yz}(i)$ and $j > i$.

Multiaxial cycle counting using the Wang and Brown is applied as follow:

1. Find the highest von Mises strain in the loading history.
2. Rearrange the loading history so that it will start the highest von Mises strain.
3. The relative von Mises strain for the whole history is then calculated using the highest von Mises strain value that was previously selected. In order to close the cycle, the highest point of the relative von Mises strain must be found.
4. So, once the highest relative von Mises strain is found and previously counted path is found, it can be considered as half cycle. The counting can be continued by following step 2 to 4.

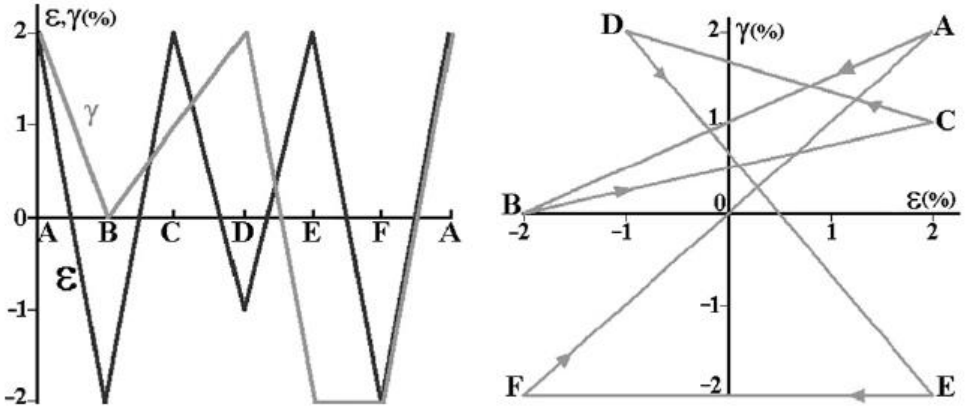

Figure 2.18 strain history for the considered NIP loading and corresponding $\gamma - \varepsilon$ diagram [52]

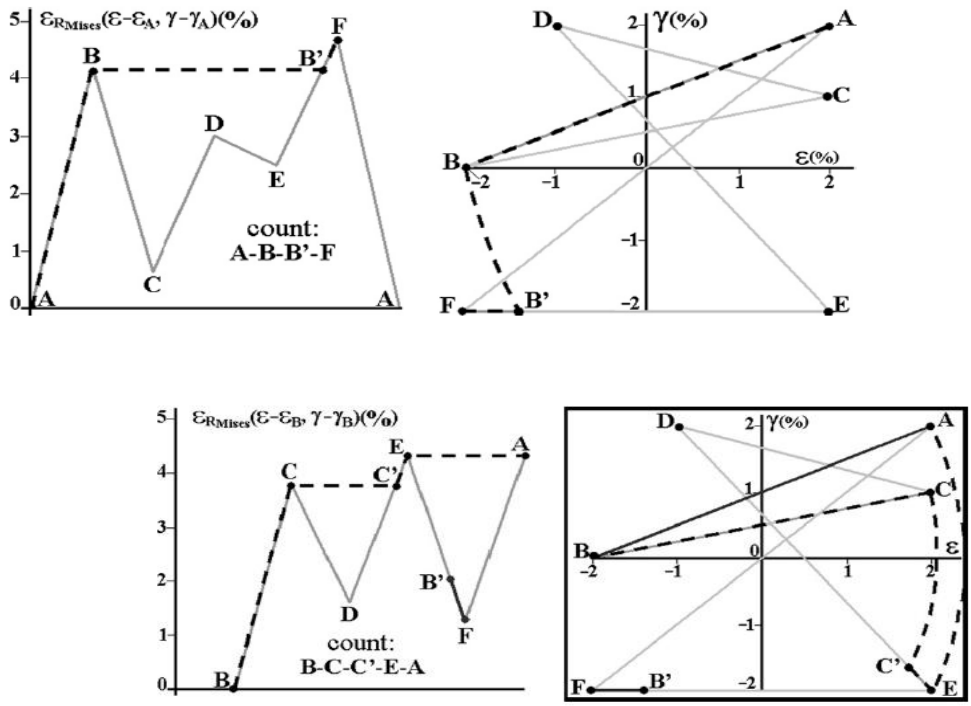

Figure 2.19 Rainflow course of the second event of the history and corresponding $\gamma - \varepsilon$ diagram [52]

The advantage in using WB method is that different from cases where loading history is random or comprises a few long blocks, cracks may propagate faster, this approach would work better as it allows the critical plane to change every reversal, which would maximise the damaged calculated. Wang and Brown underlined that Under torsional loading, it is likely that the true fatigue damage would be exaggerated by the shear damage criterion. Another problem in using this approach is that it does not predict properly the plane at which crack takes place [53].

Matus and Dominik Pointed that the Wang and Brown counting does the whole counting runs only once which means that it is less time consuming and the cycle that are extracted can be correlate with other multiaxial criteria. Even though it does the counting once it is only able to extract half –cycles[54]. Another problem associated with the WB method is that during the loading history it can ignore highest stress[55]. Wei and dong[56] noticed that the WB cycle counting method does not take into account the impact that path dependency has in fatigue damage.

2.8.2 Bannantine and Socie

In an attempt to overcome the problem associate with cycle identification in order to determine fatigue life in a multiaxial variable loading condition Bannantine and Socie proposed an approach that combines the critical plane damage parameter, Rainflow cycle counting technique with Miner's Rule damage accumulation [57]. Both Bannantine and Socie proposed that the plane that experiences the most damage is the plane at which fatigue damage takes place and it can be determined using the strain approach in the variable loading history on that same plane.

Cycles are counted using the traditional rainflow technique in the critical plane. Miner rule is then used to add up the damage contribution for a particular plane. Critical plane Socie is the plane that experiences highest damage. In Figure 2.20 the methodology behind the Bannatine and Socie method is presented.

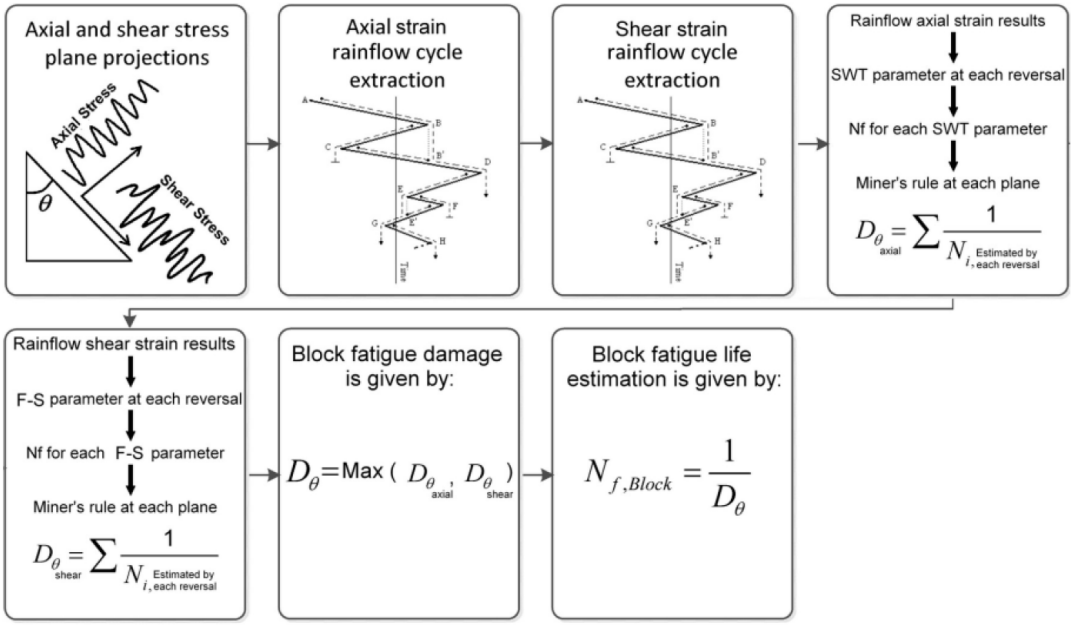

Figure 2.20 Bannantine and Socie method for multiaxial loading history.

Matus and Dominik[54] pointed that the main negative aspects of BS approach since the rainflow flow methods have to be applied to several planes makes this method very time consuming. Another drawback pointed by Anes et al [55] concerning damage characterization in BS approach is the disconnection of how much axial and shear loading components contributed to the fatigue damage.

2.8.3 Virtual cycle counting (vcc)

A new non-rainflow cycle counting method called “virtual cycle counting” was developed by Anes et al[55]. This method has its basis on the theory of SSF equivalent stress which was also developed by the same authors (see section 2.3). The physical significance of virtual cycle counting technique is based on the relationship between the maximum damage parameter in a block with its total damage. Virtual cycle counting method was developed account for variable amplitude multiaxial loading.

In Figure 2.21 the cycle counting steps behind the virtual cycle counting technique is presented together with fatigue life estimation block. From Figure 2.21 a) the variation between axial and shear components is shown. Based on this stress variation the SSF time history is constructed as shown in Figure 2.21 b). After computing the SSF time history, the shear stress value corresponding to peak stress and valley stress between successive zero stress point are identified (see Figure 2.21 c)). Figure 2.21 d) shows the block damage value which is obtained using the maximum SSF Value and this block damage value is used in determining block fatigue life estimations (see Figure 2.21 e)).

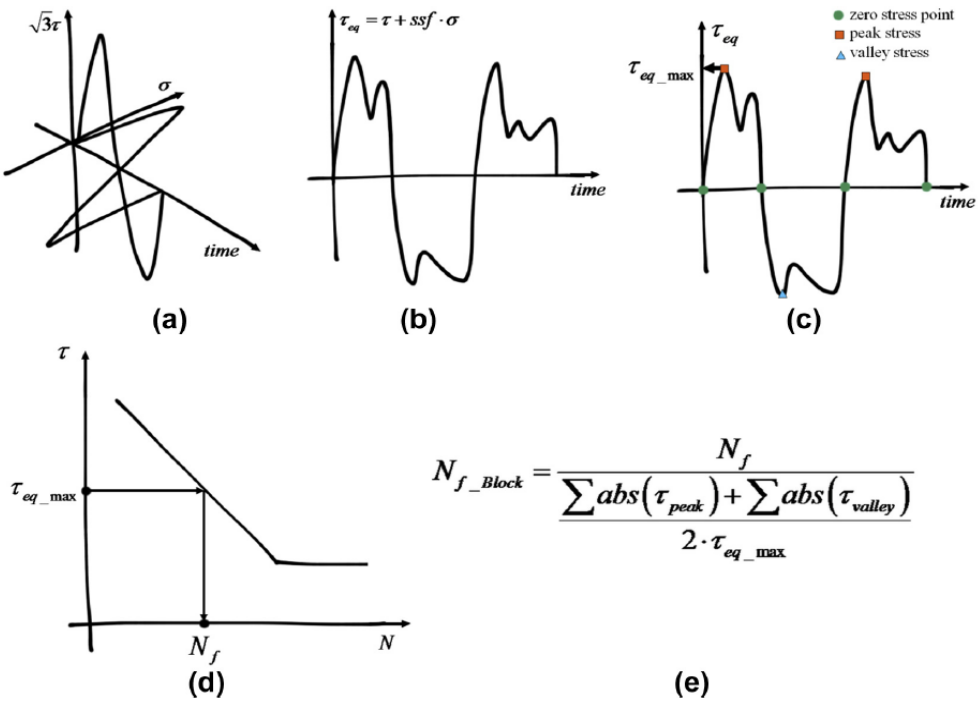

Figure 2.21 SSF virtual cycle counting process and fatigue life estimation block [55].

This approach uses an SSF function, which is a function that considers how much influence the applied load as well as the load amplitude has on fatigue strength. The SSF is calculated using Eq. (2.33).

The cycle counting is done using the following equation:

$$vcc = \frac{\sum abs(\tau)_{peak,valley}}{2.\tau_{max,Block}} \tag{2.44}$$

Where: vcc is the number of virtual cycle counted on a loading block and τ is the SSF equivalent shear stress at each peak/valley. One advantage associated with virtual cycle counting is that the theory behind it is simple and can be easily applied.

2.9 Damage accumulation

It is known that in most practical applications components are subjected to a sequence of random loads in service, and the fact that there is a random loading condition makes the analysis even more complex. It is important to mention that most data available from fatigue experiments were obtained under constant amplitude loading which is very rare in practical applications. Data are many times obtained in tests done under constant loading because fatigue experiments that are carried out with variable amplitude loading are expensive and time consuming.

To make an assessment of the damage in a material under variable loading a cycle counting technique is firstly used to extract cycles from loading history, then damage parameter to obtain the damage caused by each individual cycle is used and finally the overall damage is obtained by adding the impact caused by each cycle.

The amount of damage that a material faces is dependent on many parameters as: applied stress, number of cycles, temperature, frequency, moisture content, geometric shape of the material [58].

2.10 Linear damage rule

The concept of linear damage accumulation was first used in 1924 by Palmgren [59]. But this concept is usually attributed to Miner because of his work on tension-tension axial fatigue data for aircraft skin material in which it was demonstrated that there is good correlation between experimental data and that of linear rule [18] . But it is worth noticing that most

experimental fatigue data that are available were collected under constant load. And in reality, in most applications the loading condition is variable, which means that the loading profile is also more complex.

The idea behind the linear rule is to evaluate the contribution that each cycle has to the total damage based on fraction of the number of cycles that leads to failure at that stress/load level. Therefore, fatigue failure would occur if $D = 1$.

Miner rule is expressed by the following expression:

$$D = \sum \frac{n_i}{N_f} \tag{2.45}$$

Where: D is the total damage, n_i is the number of cycles and N_f is the number of cycles to failure.

There are many cumulative damage models available in the literature. However, amongst those Palmgren remains the most used, this is because it is simple and straightforward to use. In addition to that the results from Miner rule are in good agreement with experimental results[59]. For instance, the Linear damage rule is the most commonly used in European automotive industry [60].

However, there are some shortcomings associated with this rule. These deficiencies are: load-level independence, load-sequence independence and lack of load-interaction accountability [61].

The results estimated by Miner rule approach only take into account damage that are caused by stress greater than the fatigue limit. But, in practical applications such as industrial machines, components may damage due to cyclic load which are lower than fatigue limit (see Figure 2.22). Cumulative damage at failure substantially decreased down D=0.001 when η was small**.** According Kondo [62] the probable cause for this discrepancy is that the Miner rule did not consider stress below the fatigue limit.

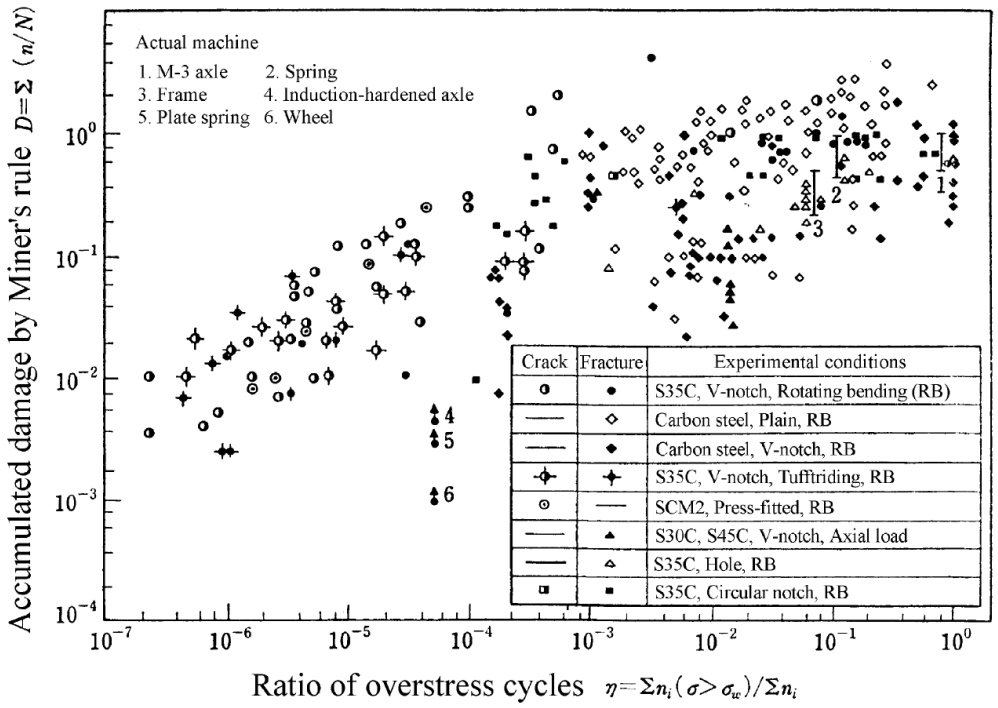

Figure 2.22 Linear cumulative damage model for experimental and actual machines [62].

Concerning the load sequence, the damage sum to failure is greater than unity for low-high tests and less than unity for high-low tests [58]. This means that if there is loading block that goes from high to low fatigue failure would take place at lower cumulative damage whereas from low to high it would occur at higher cumulative damage.

Even though many nonlinear cumulative damage models were proposed, the Linear damage rules continue to be the most used. In the literature, many of the disadvantages in estimating fatigue damage that are associated with linear damage rule are due to the use of an unsuitable damage parameter rather than due to linear damage rule.[16]. Even though there are many shortcomings associated with it and it cannot also capture fully the behaviour of material under variable loading, Miner Rule continues to be widely used in analysis of variable loading fatigue due to its simplicity.

2.11 Practical example of cycle counting and damage accumulation usage

In order to assess the fatigue life of a component under variable loading amplitude Palmgren-Miner damage accumulation rule is usually combined with S-N curves [63] The load time history that is generated in most practical applications is complex and irregular, because of that the fatigue analysis becomes harder due to the limitations associated with current

theories and technologies. To accurately determine how much damage a particular component has suffered an efficient cycle counting method must be employed in order to accurately identify the number of cycles. If the cycle is not properly recorded there will be a loss of information which will affect the overall fatigue analysis.

There are many cycle counting techniques but the rainflow method developed by the Endo and Matsuishi remains as the most used. However, the algorithm that was proposed by the original rainflow technique is very complex and today it is often used as the rainflow count rather than a way to find cycles. Today, out of many algorithms that are based on the rainflow two are mostly used, 3-point algorithm that was proposed by Downing and Socie [40] as well as 4-point algorithm . From these algorithms it is expected that full and half cycle are properly captured. Concerning to the identification of cycle, an offline or an online rainflow can be used. The offline method is used in applications which the applying load is random, but it is worth mentioning that at its original form the offline method becomes impractical if used in real time situation.

The drawback of using an offline rainflow is that it requires a lot of computational resources because the entire stored data have to be processed at the same time and this means that life estimates results will only be updated at the end of each block. In applications which using offline technique will not yield accurate life estimation, it is advised to use the real time rainflow algorithm. The advantage of using real time rainflow instead of offline method is that with the online method each cycle or half-cycle is extracted from the loading history as it happens. Thus, the online approach also requires less storage memory which will be more efficient computationally [64].

An aircraft, a car, a helicopter or any other means of transportation must go through a maintenance between certain number of working hours (service operation), this is done to ensure that the aircraft is safe to operate again. But it is important to highlight that sometimes aircraft fail even without any probable sign of failing. Because of that real time monitoring is very important to make sure that aircraft is operating safely.

2.11.1 Fatigue life monitoring

The process that is commonly used to assess the amount of damage that a component has suffered is known as Operational Loads Monitoring (OLM). The implementation of OLM in aircraft is usually done using two techniques such as: The flight parameters-based loads monitoring and strain gauge-based loads monitoring.

The flight parameters-based loads monitoring technique is done using the sensors that are placed in the aircraft during manufacture, these sensors are used to measure flight parameters as speed, acceleration, mass, altitude, etc. The loading is then estimated using the data collected by the sensors. Since the loads are not directly measured this method fails to provide the required precision to estimate fatigue life [65]. The other issue associated with this method is that it is expensive. Because of the lack of precision that the previous method has, aircraft manufacture started using the system based on strain gauge which it is placed on chosen location. In this method, for the various strain gauge placed in different locations, monitoring of strain sequences is performed, data is stored in DAU (data acquisition unit) and this same data is downloaded between specific intervals.

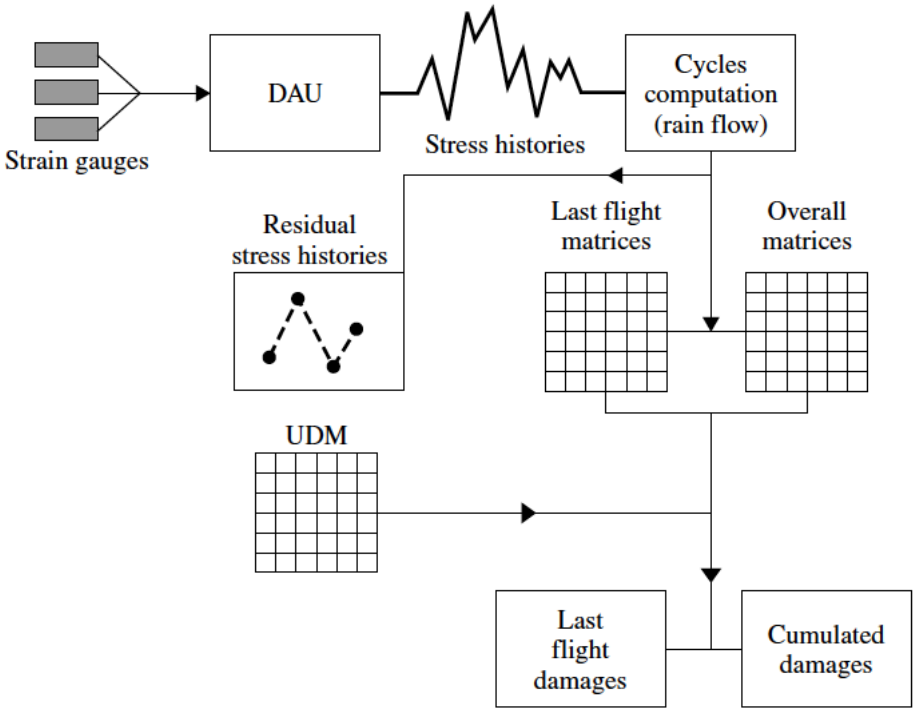

Figure 2.23 Loads monitoring system using strain gauge for Tornado aircraft [65].

From Figure 2.23, the strain information in the sensors are transformed into a digital signals and then stored in DAU. These digital signals are also converted into stress histories so that the load sequence in different parts could be obtained. Once the load sequence is obtained, the traditional rainflow counting method is applied in order to do the analysis and this process can be performed both during flight or on the ground.

Using a fatigue – life (S–N) curve for the material and notch considered as well as a damage accumulation rule allows determining a Fatigue Index (FI), which is nothing more than the estimated accumulated damage. The extent of fatigue damage induced by m blocks of constant σ_i stress amplitudes can be estimated using the well-known Palmgren–Miner damage accumulation rule, see Eq. (2.46), which states that failure will occur when:

$$\sum_{i=1}^{m} \frac{n_i}{N_f} = 1 \tag{2.46}$$

Where: $n_i$is the number of fatigue cycles corresponding to each block of load and N_f is the number of fatigue cycles to failure at the amplitude stress level σ_i.

3. SSF damage map

It was done a literature review regarding multiaxial models and multiaxial damage accumulation and several questions arise about the stress scale factor (SSF) methodology regarding the plane in which the respective damage map is evaluated.

In this chapter, the influence of the plane evaluation in the fatigue life estimates was studied and it was also evaluated the SSF damage map for several orientations and the results correlated with the critical plane approaches.

The main idea is to explain and discuss why the critical plane models have such poor results regarding fatigue life estimates. It was considered experimental data found in literature regarding experimental critical planes of the high strength steel 42CrMo4 and then it was evaluated the SSF damage map on that critical plane orientations, it was found that the damage map changes according with the critical plane orientations which is the reason that justifies the poor performance of these models because they have a constant damage scale between shear and normal stresses but in reality this scale changes according to the plane of evaluation, which is confirmed in this study.

3.1 Material and loading paths

The material used in this study was the high strength steel 42CrMo4, its monotonic and cyclic mechanical properties are shown in Table 3.2 and previously determined using ASTM E8 and ASTM E606 standards [23]. This material is used to manufacture a variety of automotive components namely front vehicle axles, steering components, crankshafts and hot forging components. The chemical composition of 42CrMo4 is shown in Table 3.1

Table 3.1 42CrMo4 chemical composition [33].

Element	C	Si	Mn	P	S	Cr	Ni	Mo	Cu
Weight (%)	0.39	0.17	0.77	0.025	0.02	1.1	0.3	0.16	0.21

Table 3.2 Monotonic and cyclic mechanical properties of 42 CrMo4 [23].

	42CrMo4
Microstructure type	bcc
Poisson's ratio	0.3
Density (Kg/m^3)	7830
Hardness (HV)	362
Tensile strength (MPa)	1100
Yield strength (MPa)	980
Young's modulus(GPa)	206
Elongation (%)	16
$\sigma_f^{'}$ **Fatigue strength coeficient (MPa)**	1154
b **Fatigue strength coefficient**	-0.061
$\varepsilon_f^{'}$**Fatigue ductility coefficient**	0.180
c **Fatigue ductility exponent**	-0.53

Five different proportional loading paths shown in Figure 3.1 were considered for this study.The first two loading paths are uniaxial pure normal and pure shear and the rest are proportional loading with different stress amplitude ratios.

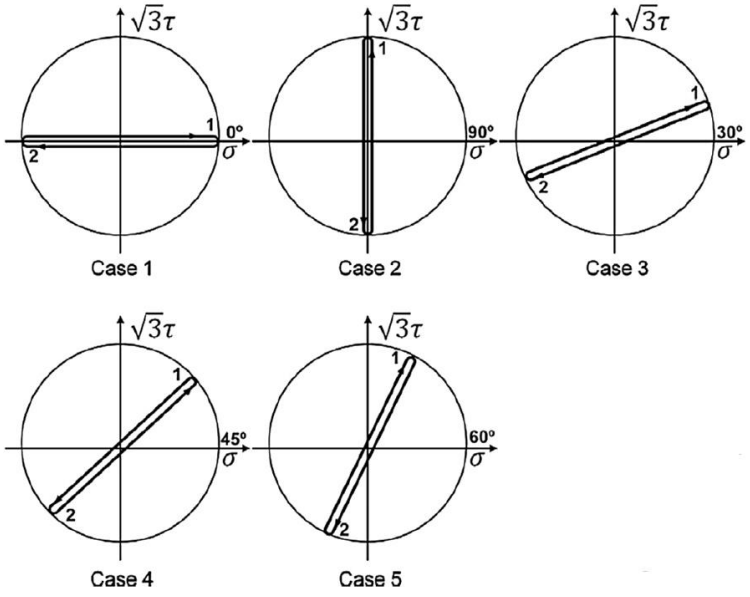

Figure 3.1 Loading paths. Case 1-pure tension, case 2 – pure shear. Case 3 – proportional loading with stress amplitude ratio equal to 30°, Case 4 – proportional loading with stress amplitude ratio equal to 45°, Case 5 – proportional loading with stress amplitude ratio equal to 60°[33].

3.2 Graphical representation of SSF results

The SSF results that are presented in Annex A.1 were evaluated at 0°. In this study, the analysis were extended to others plane orientations starting from -90° to 90°. In order to do the analysis, the SSF values for -90° to 90° for each loading path shown in Figure 3.1(excepting PS case) were estimated and those results are shown in table 3.3 to 3.6.

Table 3.3 The SSF results evaluated from -90°to 90° for PT.

Ciclos	Graus	-90	-85	-80	-75	-70	-65	-60	-55	-50	-45	-40	-35	-30	-25	-20	-15	-10	-5	0	5	10	15	20	25	30	35	40	45	50	55	60	65	70	75	80	85	90
1000	axial	0	25	39	41	32	11	20	62	112	169	231	297	364	431	495	554	607	652	688	713	727	729	720	699	668	626	576	519	457	391	324	257	193	134	81	36	0
	corte	0	60	118	172	221	264	298	323	339	344	339	323	298	264	221	172	118	60	0	60	118	172	221	264	298	323	339	344	339	323	298	264	221	172	118	60	0
	corte uniaxial	567																																				
	Delta	567	507	449	395	346	303	269	244	228	223	228	244	269	303	346	395	449	507	567	507	449	395	346	303	269	244	228	223	228	244	269	303	346	395	449	507	567
	ssf	2.64E+16	20.16	11.49	9.54	10.81	27.15	13.16	3.94	2.04	1.32	0.99	0.82	0.74	0.70	0.70	0.71	0.74	0.78	0.82	0.71	0.62	0.54	0.48	0.43	0.40	0.39	0.40	0.43	0.50	0.62	0.83	1.18	1.79	2.96	5.58	14.24	2.64E+16
10000	axial	0	5	18	40	70	107	150	198	248	301	353	403	451	494	531	561	583	596	601	596	583	561	531	494	451	403	353	301	248	198	150	107	70	40	18	5	0
	corte	0	52	103	150	193	230	260	282	296	301	296	282	260	230	193	150	103	52	0	52	103	150	193	230	260	282	296	301	296	282	260	230	193	150	103	52	0
	corte uniaxial	493																																				
	Delta	493	441	390	343	300	263	233	211	197	193	197	211	233	263	300	343	390	441	493	441	390	343	300	263	233	211	197	193	197	211	233	263	300	343	390	441	493
	ssf	N/A	96.56	21.53	8.51	4.26	2.45	1.55	1.07	0.79	0.64	0.56	0.52	0.52	0.53	0.56	0.61	0.67	0.74	0.82	0.74	0.67	0.61	0.56	0.53	0.52	0.52	0.56	0.64	0.79	1.07	1.55	2.45	4.26	8.51	21.53	96.56	N/A
100000	axial	0	4	16	35	61	94	131	172	217	262	307	352	393	430	463	489	508	520	524	520	508	489	463	430	393	352	307	262	217	172	131	94	61	35	16	4	0
	corte	0	45	90	131	168	201	227	246	258	262	258	246	227	201	168	131	90	45	0	45	90	131	168	201	227	246	258	262	258	246	227	201	168	131	90	45	0
	corte uniaxial	428																																				
	Delta	428	383	338	297	260	227	201	182	170	166	170	182	201	227	260	297	338	383	428	383	338	297	260	227	201	182	170	166	170	182	201	227	260	297	338	383	428
	ssf	N/A	96.10	21.42	8.46	4.23	2.43	1.54	1.05	0.79	0.63	0.55	0.52	0.51	0.53	0.56	0.61	0.67	0.74	0.82	0.74	0.67	0.61	0.56	0.53	0.51	0.52	0.55	0.63	0.79	1.05	1.54	2.43	4.23	8.46	21.42	96.10	N/A
1000000	axial	0	3	14	31	54	82	115	151	189	229	269	307	344	376	404	427	444	455	458	455	444	427	404	376	344	307	269	229	189	151	115	82	54	31	14	3	0
	corte	0	40	78	115	147	175	198	215	226	229	226	215	198	175	147	115	78	40	0	40	78	115	147	175	198	215	226	229	226	215	198	175	147	115	78	40	0
	corte uniaxial	372																																				
	Delta	372	332	294	258	225	197	174	157	146	143	146	157	174	197	225	258	294	332	372	332	294	258	225	197	174	157	146	143	146	157	174	197	225	258	294	332	372
	ssf	N/A	95.50	21.26	8.39	4.20	2.40	1.52	1.04	0.77	0.62	0.55	0.51	0.51	0.52	0.56	0.60	0.66	0.73	0.81	0.73	0.66	0.60	0.56	0.52	0.51	0.51	0.55	0.62	0.77	1.04	1.52	2.40	4.20	8.39	21.26	95.50	N/A
1E+07	axial	0	3	12	27	47	71	100	132	165	200	235	268	300	329	353	373	388	397	400	397	388	373	353	329	300	268	235	200	165	132	100	71	47	27	12	3	0
	corte	0	35	68	100	129	153	173	188	197	200	197	188	173	153	129	100	68	35	0	35	68	100	129	153	173	188	197	200	197	188	173	153	129	100	68	35	0
	corte uniaxial	324																																				
	Delta	324	289	256	224	195	171	151	136	127	124	127	136	151	171	195	224	256	289	324	289	256	224	195	171	151	136	127	124	127	136	151	171	195	224	256	289	324
	ssf	N/A	95.20	21.19	8.36	4.18	2.39	1.51	1.03	0.77	0.62	0.54	0.51	0.50	0.52	0.55	0.60	0.66	0.73	0.81	0.73	0.66	0.60	0.55	0.52	0.50	0.51	0.54	0.62	0.77	1.03	1.51	2.39	4.18	8.36	21.19	95.20	N/A

Table 3.4 The SSF results evaluated from -90°to 90° for PP30.

Ciclos	Graus	-90	-85	-80	-75	-70	-65	-60	-55	-50	-45	-40	-35	-30	-25	-20	-15	-10	-5	0	5	10	15	20	25	30	35	40	45	50	55	60	65	70	75	80	85	90
1000	axial	0	33	55	66	64	51	26	10	55	109	169	234	302	371	438	503	561	613	656	689	711	722	720	707	682	646	601	547	487	422	354	285	218	153	95	43	0
	corte	219	159	94	26	43	110	175	233	285	328	361	383	394	392	379	354	318	273	219	159	94	26	43	110	175	233	285	328	361	383	394	392	379	354	318	273	219
	corte uniaxial	567																																				
	Delta	348	408	473	541	524	457	392	334	282	239	206	184	173	175	188	213	249	294	348	408	473	541	524	457	392	334	282	239	206	184	173	175	188	213	249	294	348
	ssf	1.30E+16	12.36	8.59	8.26	8.18	9.02	15.29	33.29	5.09	2.19	1.22	0.78	0.57	0.47	0.43	0.42	0.44	0.48	0.53	0.59	0.67	0.75	0.73	0.65	0.58	0.52	0.47	0.44	0.42	0.44	0.49	0.61	0.87	1.39	2.63	6.84	1.30E+16
10000	axial	0	29	49	58	57	45	23	9	49	97	150	208	268	329	389	446	498	544	582	611	631	640	639	627	605	573	533	485	432	374	314	253	193	136	84	38	0
	corte	194	141	83	23	38	98	155	207	253	291	320	340	349	348	336	314	282	242	194	141	83	23	38	98	155	207	253	291	320	340	349	348	336	314	282	242	194
	corte uniaxial	493																																				
	Delta	299	352	410	470	455	395	338	286	240	202	173	153	144	145	157	179	211	251	299	352	410	470	455	395	338	286	240	202	173	153	144	145	157	179	211	251	299
	ssf	1.26E+16	12.04	8.41	8.11	8.03	8.84	15.02	31.17	4.86	2.08	1.15	0.74	0.54	0.44	0.40	0.40	0.42	0.46	0.51	0.58	0.65	0.74	0.71	0.63	0.56	0.50	0.45	0.42	0.40	0.41	0.46	0.58	0.82	1.32	2.52	6.60	1.26E+16
100000	axial	0	26	43	51	50	40	20	8	44	86	133	185	238	292	345	395	442	482	516	542	559	567	566	556	536	508	472	430	383	331	278	224	171	121	74	34	0
	corte	172	125	73	20	34	87	137	184	224	258	284	301	309	308	298	278	250	214	172	125	73	20	34	87	137	184	224	258	284	301	309	308	298	278	250	214	172
	corte uniaxial	428																																				
	Delta	256	303	355	408	394	341	291	244	204	170	144	127	119	120	130	150	178	214	256	303	355	408	394	341	291	244	204	170	144	127	119	120	130	150	178	214	256
	ssf	1.21E+16	11.69	8.20	7.93	7.85	8.61	14.56	30.05	4.65	1.98	1.08	0.69	0.50	0.41	0.38	0.38	0.40	0.44	0.50	0.56	0.63	0.72	0.70	0.61	0.54	0.48	0.43	0.40	0.38	0.38	0.43	0.54	0.76	1.24	2.39	6.33	1.21E+16
1000000	axial	0	23	39	46	45	35	18	7	39	76	118	164	211	259	306	351	392	428	458	481	497	504	503	493	476	451	419	382	340	294	247	199	152	107	66	30	0
	corte	153	111	65	18	30	77	122	163	199	229	252	268	275	274	264	247	222	190	153	111	65	18	30	77	122	163	199	229	252	268	275	274	264	247	222	190	153
	corte uniaxial	372																																				
	Delta	219	261	307	354	342	295	250	209	173	143	120	104	97	98	108	125	150	182	219	261	307	354	342	295	250	209	173	143	120	104	97	98	108	125	150	182	219
	ssf	1.17E+16	11.31	7.96	7.73	7.64	8.33	13.90	30.29	4.49	1.88	1.02	0.64	0.46	0.38	0.35	0.36	0.38	0.42	0.48	0.54	0.62	0.70	0.68	0.60	0.53	0.46	0.41	0.37	0.35	0.35	0.39	0.49	0.71	1.17	2.27	6.04	1.17E+16
10000000	axial	0	20	34	40	39	31	15	7	35	68	105	146	188	230	272	311	348	379	406	426	440	446	445	437	421	399	371	338	301	260	218	176	134	95	58	27	0
	corte	135	98	57	15	27	69	108	145	176	203	223	237	243	242	234	218	196	168	135	98	57	15	27	69	108	145	176	203	223	237	243	242	234	218	196	168	135
	corte uniaxial	324																																				
	Delta	189	226	267	309	297	255	216	179	148	121	101	87	81	82	90	106	128	156	189	226	267	309	297	255	216	179	148	121	101	87	81	82	90	106	128	156	189
	ssf	1.14E+16	11.12	7.86	7.66	7.56	8.26	13.99	26.73	4.24	1.78	0.96	0.60	0.43	0.36	0.33	0.34	0.37	0.41	0.47	0.53	0.61	0.69	0.67	0.58	0.51	0.45	0.40	0.36	0.33	0.33	0.37	0.46	0.67	1.11	2.19	5.87	1.14E+16

Table 3.5 The SSF results evaluated from -90°to 90° for PP45.

Ciclos	Graus	-90	-85	-80	-75	-70	-65	-60	-55	-50	-45	-40	-35	-30	-25	-20	-15	-10	-5	0	5	10	15	20	25	30	35	40	45	50	55	60	65	70	75	80	85	90
1000	axial	0	60	109	144	165	171	162	139	101	50	12	84	163	247	333	419	502	580	650	710	759	794	815	821	812	789	751	700	638	566	487	403	317	231	148	70	0
	corte	375	313	241	162	78	8	94	177	255	325	385	434	469	490	496	487	464	426	375	313	241	162	78	8	94	177	255	325	385	434	469	490	496	487	464	426	375
	corte uniaxial	567																																				
	Delta	192	254	326	405	489	559	473	390	312	242	182	133	98	77	71	80	103	141	192	254	326	405	489	559	473	390	312	242	182	133	98	77	71	80	103	141	192
	ssf	4.18E+15	4.22	3.00	2.81	2.96	3.27	2.92	2.81	3.10	4.84	14.99	1.59	0.60	0.31	0.21	0.19	0.21	0.24	0.30	0.36	0.43	0.51	0.60	0.68	0.58	0.49	0.42	0.35	0.29	0.24	0.20	0.19	0.22	0.35	0.70	2.02	4.18E+15
10000	axial	0	52	94	124	142	148	140	120	88	44	9	71	139	211	285	359	431	498	558	610	652	682	700	706	698	678	646	602	549	487	419	347	273	199	127	60	0
	corte	323	270	208	140	68	6	80	152	219	279	331	373	403	421	427	419	399	367	323	270	208	140	68	6	80	152	219	279	331	373	403	421	427	419	399	367	323
	corte uniaxial	493																																				
	Delta	105	158	220	288	360	422	348	276	209	149	97	55	25	7	1	9	29	61	105	158	220	288	360	422	348	276	209	149	97	55	25	7	1	9	29	61	105
	ssf	2.65E+15	3.05	2.35	2.32	2.53	2.86	2.48	2.30	2.39	3.39	10.38	0.78	0.18	0.03	0.00	0.02	0.07	0.12	0.19	0.26	0.34	0.42	0.51	0.60	0.50	0.41	0.32	0.25	0.18	0.11	0.06	0.02	0.00	0.04	0.23	1.02	2.65E+15
100000	axial	0	44	80	106	122	126	120	102	74	37	9	62	120	182	246	309	371	428	480	524	560	586	602	606	600	582	554	517	471	418	360	298	234	171	109	52	0
	corte	277	231	178	120	58	6	69	131	188	240	284	320	346	362	366	360	342	314	277	231	178	120	58	6	69	131	188	240	284	320	346	362	366	360	342	314	277
	corte uniaxial	428																																				
	Delta	216	262	315	373	435	487	424	362	305	253	209	173	147	131	127	133	151	179	216	262	315	373	435	487	424	362	305	253	209	173	147	131	127	133	151	179	216
	ssf	6.36E+15	5.89	3.92	3.51	3.57	3.85	3.53	3.54	4.09	6.84	23.47	2.80	1.22	0.72	0.51	0.43	0.41	0.42	0.45	0.50	0.56	0.64	0.72	0.80	0.71	0.62	0.55	0.49	0.44	0.41	0.41	0.44	0.54	0.78	1.38	3.45	6.36E+15
1000000	axial	0	38	69	91	105	109	103	88	64	32	7	53	103	156	211	265	318	368	412	450	481	503	517	521	515	500	476	444	405	359	309	256	201	147	94	44	0
	corte	238	199	153	103	50	5	59	112	162	206	244	275	297	311	315	309	294	270	238	199	153	103	50	5	59	112	162	206	244	275	297	311	315	309	294	270	238
	corte uniaxial	372																																				
	Delta	134	173	219	269	322	367	313	260	210	166	128	97	75	61	57	63	78	102	134	173	219	269	322	367	313	260	210	166	128	97	75	61	57	63	78	102	134
	ssf	4.60E+15	4.54	3.17	2.94	3.07	3.38	3.03	2.95	3.28	5.19	17.30	1.84	0.73	0.39	0.27	0.24	0.24	0.28	0.33	0.39	0.45	0.53	0.62	0.71	0.61	0.52	0.44	0.37	0.32	0.27	0.24	0.24	0.28	0.43	0.83	2.29	4.60E+15
10000000	axial	0	33	59	78	90	93	88	75	55	27	7	46	89	135	181	228	274	316	354	387	413	432	444	447	442	429	409	381	347	308	265	219	173	126	80	38	0
	corte	204	170	131	88	42	4	51	97	139	177	210	236	255	267	270	265	252	232	204	170	131	88	42	4	51	97	139	177	210	236	255	267	270	265	252	232	204
	corte uniaxial	324																																				
	Delta	120	154	193	236	282	320	273	227	185	147	114	88	69	57	54	59	72	92	120	154	193	236	282	320	273	227	185	147	114	88	69	57	54	59	72	92	120
	ssf	4.80E+15	4.70	3.26	3.01	3.14	3.43	3.09	3.02	3.39	5.44	16.72	1.92	0.77	0.43	0.30	0.26	0.26	0.29	0.34	0.40	0.47	0.55	0.63	0.71	0.62	0.53	0.45	0.39	0.33	0.29	0.26	0.26	0.31	0.47	0.89	2.42	4.80E+15

Table 3.6 The SSF results evaluated from -90°to 90° for PP60.

Ciclos	Graus	-90	-85	-80	-75	-70	-65	-60	-55	-50	-45	-40	-35	-30	-25	-20	-15	-10	-5	0	5	10	15	20	25	30	35	40	45	50	55	60	65	70	75	80	85	90
1000	axial	0	84	158	220	267	298	313	310	290	254	202	136	59	28	122	220	319	416	508	592	666	728	775	806	821	818	798	762	710	644	567	480	386	288	189	92	0
	corte	508	456	390	313	226	132	34	65	162	254	338	412	474	521	552	567	564	544	508	456	390	313	226	132	34	65	162	254	338	412	474	521	552	567	564	544	508
	corte uniaxial	567																																				
	Delta	59	111	177	254	341	435	533	502	405	313	229	155	93	46	15	0	3	23	59	111	177	254	341	435	533	502	405	313	229	155	93	46	15	0	3	23	59
	ssf	9.48E+14	1.31	1.11	1.15	1.28	1.46	1.70	1.62	1.39	1.23	1.13	1.13	1.58	1.63	0.12	0.00	0.01	0.05	0.12	0.19	0.26	0.35	0.44	0.54	0.65	0.61	0.51	0.41	0.32	0.24	0.16	0.10	0.04	0.00	0.01	0.25	9.48E+14
10000	axial	0	65	121	168	205	229	240	238	222	195	155	105	45	22	93	168	244	318	389	454	510	557	594	618	629	627	611	584	544	494	434	367	296	221	145	71	0
	corte	389	349	299	240	173	101	26	50	124	195	259	316	363	399	423	434	432	417	389	349	299	240	173	101	26	50	124	195	259	316	363	399	423	434	432	417	389
	corte uniaxial	493																																				
	Delta	104	144	194	253	320	392	467	443	369	299	234	177	130	94	70	59	61	76	104	144	194	253	320	392	467	443	369	299	234	177	130	94	70	59	61	76	104
	ssf	2.18E+15	2.22	1.60	1.50	1.56	1.72	1.95	1.87	1.66	1.53	1.51	1.70	2.88	4.36	0.75	0.35	0.25	0.24	0.27	0.32	0.38	0.45	0.54	0.63	0.74	0.71	0.60	0.51	0.43	0.36	0.30	0.26	0.24	0.27	0.42	1.08	2.18E+15
100000	axial	0	49	93	129	157	175	184	182	170	149	119	80	35	16	72	129	187	244	298	347	391	427	455	473	482	480	468	447	417	378	333	282	226	169	111	54	0
	corte	298	268	229	184	133	77	20	38	95	149	198	242	278	306	324	333	331	319	298	268	229	184	133	77	20	38	95	149	198	242	278	306	324	333	331	319	298
	corte uniaxial	428																																				
	Delta	130	160	199	244	295	351	408	390	333	279	230	186	150	122	104	95	97	109	130	160	199	244	295	351	408	390	333	279	230	186	150	122	104	95	97	109	130
	ssf	3.56E+15	3.24	2.14	1.89	1.89	2.00	2.22	2.14	1.95	1.87	1.94	2.32	4.34	7.42	1.45	0.74	0.52	0.45	0.44	0.46	0.51	0.57	0.65	0.74	0.85	0.81	0.71	0.62	0.55	0.49	0.45	0.43	0.46	0.56	0.87	2.01	3.56E+15
1000000	axial	0	38	71	99	120	134	140	139	130	114	91	61	26	13	55	99	143	187	228	266	299	327	348	362	368	367	358	342	319	289	254	215	173	129	85	41	0
	corte	228	205	175	140	101	59	15	29	73	114	152	185	213	234	248	254	253	244	228	205	175	140	101	59	15	29	73	114	152	185	213	234	248	254	253	244	228
	corte uniaxial	372																																				
	Delta	144	167	197	232	271	313	357	343	299	258	220	187	159	138	124	118	119	128	144	167	197	232	271	313	357	343	299	258	220	187	159	138	124	118	119	128	144
	ssf	5.16E+15	4.42	2.77	2.35	2.26	2.34	2.54	2.46	2.30	2.26	2.43	3.05	6.02	10.94	2.27	1.19	0.83	0.68	0.63	0.63	0.66	0.71	0.78	0.86	0.97	0.93	0.84	0.75	0.69	0.65	0.63	0.64	0.72	0.91	1.40	3.09	5.16E+15
10000000	axial	0	29	55	76	92	103	108	107	100	88	70	47	20	10	42	76	110	143	175	204	230	251	267	278	283	282	275	263	245	222	195	165	133	99	65	32	0
	corte	175	157	135	108	78	45	12	22	56	88	117	142	163	180	190	195	194	188	175	157	135	108	78	45	12	22	56	88	117	142	163	180	190	195	194	188	175
	corte uniaxial	324																																				
	Delta	149	167	189	216	246	279	312	302	268	237	207	182	161	144	134	129	130	136	149	167	189	216	246	279	312	302	268	237	207	182	161	144	134	129	130	136	149
	ssf	6.95E+15	5.74	3.47	2.85	2.68	2.71	2.90	2.82	2.68	2.70	2.98	3.87	7.92	14.92	3.18	1.70	1.18	0.95	0.85	0.82	0.83	0.86	0.92	1.00	1.10	1.07	0.98	0.90	0.85	0.82	0.82	0.87	1.01	1.30	1.99	4.30	6.95E+15

The estimated SSF values were plot against plane orientation (see Fig.(s) 3.2 to 3.5), However, as shown in Fig.(s) 3.2 to 3.5, it was only considered plane orientation that starts from -75° to 75°. This is because for other orientations the SSF values become too large.

To make the SSF variation visible, for each loading path instead of showing the SSF variation in one figure only, two figures with different scales were considered for each case. From Fig.(s) 3.2 to 3.5, each of the colour represent a particular number of cycles. These figures show how the SSF vary with plane orientations and fatigue life for each of the loading paths.

For a pure tension case shown in Figure 3.2, it can be observed that the SSF parameter varies with plane orientation. However, for some of the orientations the SSF is almost the same even though the fatigue life is different. However, for the proportional loading cases (Fig.(s) 3.3 to 3.5) due the presence of shear component it can be observed that the SSF evolution becomes more chaotic from one loading case to another.

PT

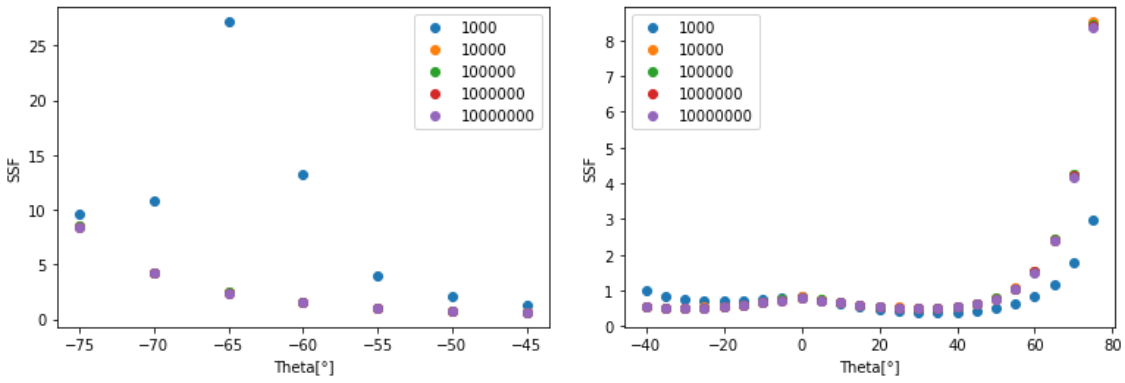

(a) (b)

Figure 3.2 SSF evolution with plane orientation and number of cycles for PT: (a) -75° to 45° and (b) -40° to 75°.

PP30

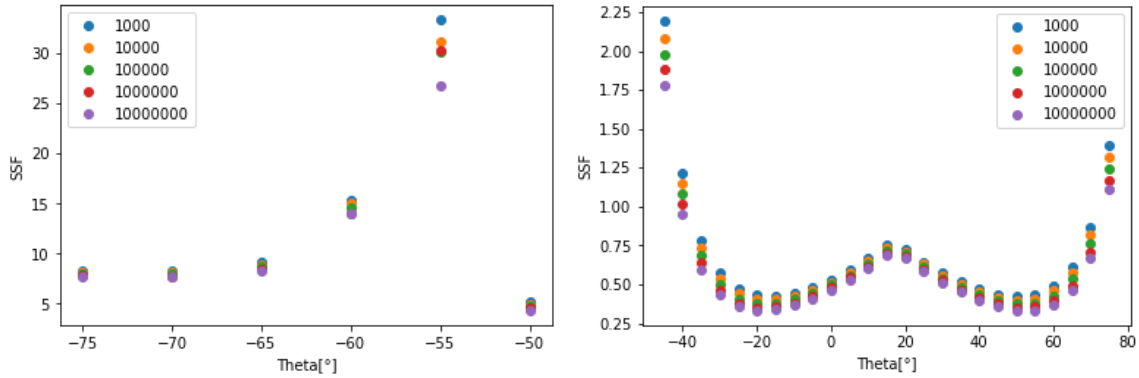

(a) (b)

Figure 3.3 SSF evolution with plane orientation and number of cycles for PP30: (a) -75° to -50° and (b) -45° to 75°.

For instance, it is possible to see that the SSF evolution for PP45 is much more disperse than for PP30 (see Figure 3.3 and 3.4) and it can also be observed that for PP60 the SSF variation is even more disperse than both PP30 and PP45 loading paths, this happens because from PP30, PP45 to PP60 the shear percentage increases while the axial decreases. It is also known that shear component has an increased damaged compared to axial component. This result also confirms that there is a damage scale between normal and shear stresses according to the loading path considered.

PP45

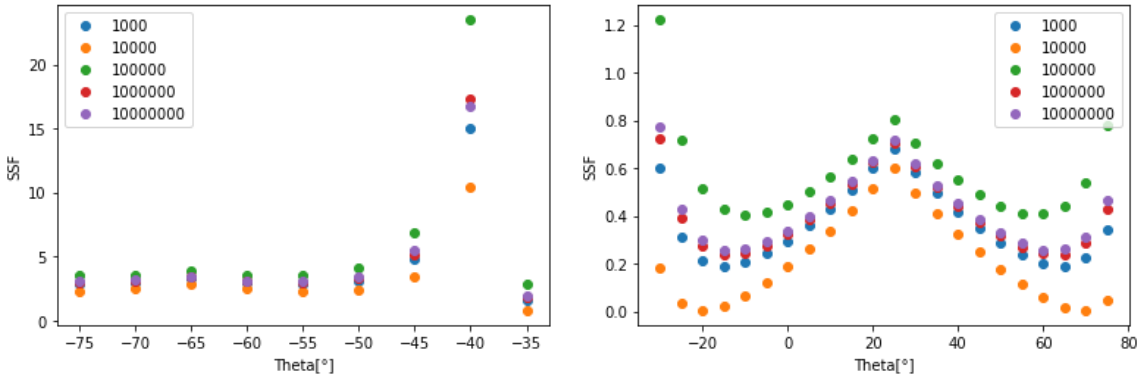

(a) (b)

Figure 3.4 SSF evolution with plane orientation and number of cycles for PP45: (a) -75° to -35° and (b) -30° to 75°.

PP60

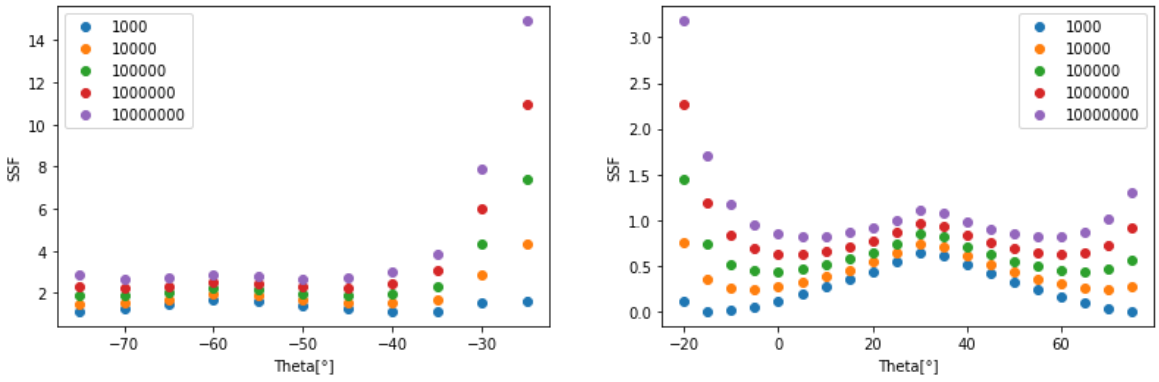

(a) (b)

Figure 3.5 SSF evolution with plane orientation and number of cycles for PP60: (a) -75° to -25° and (b) -20° to 75°.

Based on Fig.(s) 3.2 to 3.5 it was proved that the damage scale parameter in fact changes with loading plane orientation. This damage scale variation with plane direction is the reason

why critical plane models predicts poor fatigue results, that is because in critical plane approach the damage scale is usually seen as material property which means that it is a constant value.

3.3 SSF surface plot

The experimental data needed to obtain SSF surface is shown in Table 3.7. These results were obtained using trend line equations that represents different loading case (see Annex A.2). From Table 3.7, the first five data represent the PT loading case, and the following represent PP30, PP45, PP60 and PS respectively.

To obtain the SSF shown in Figure 3.6 a software called Datafit was used. Datafit is a software which contains several functions in its database so that when the regression is performed, it will generate several surfaces in numerical order, this numerical order depends on the R^2 value this means that the surface with the R^2 closer to 1 will be in the first position. However, the SSF surface is selected from results not only according to R^2 value but it is also checked if the surface evolution corresponds to fatigue physical phenomenon.

Using the experimental data presented in Table 3.7, the SSF surface shown in Figure 3.6 was obtained with an $R^2 = 0.98$ and it is represented by the Eq. (3.1).

Table 3.7 Experimental data used to obtain SSF surface for 0-degree orientation[33].

$\sigma_a(MPa)$	$\lambda\ (rad)$	SSF
688	0	0.77
601	0	0.79
524	0	0.81
458	0	0.82
400	0	0.84
656	0.32	0.53
582	0.32	0.51
516	0.32	0.50
458	0.32	0.48
406	0.32	0.46
650	0.52	0.30
558	0.52	0.31
480	0.52	0.32
412	0.52	0.33
354	0.52	0.34
508	0.79	0.12
389	0.79	0.27
298	0.79	0.44
228	0.79	0.63
175	0.79	0.85
0	0	0.38
0	0	0.39
0	0	0.40
0	0	0.41
0	0	0.42

$$SSF(\sigma_a, \lambda) = a + b\sigma_a + c\sigma_a^2 + d\sigma_a^3 + f\lambda^2 + \mathrm{g}\lambda^3 + \mathrm{h}\lambda^4 + i\lambda^5 \qquad (3.1)$$

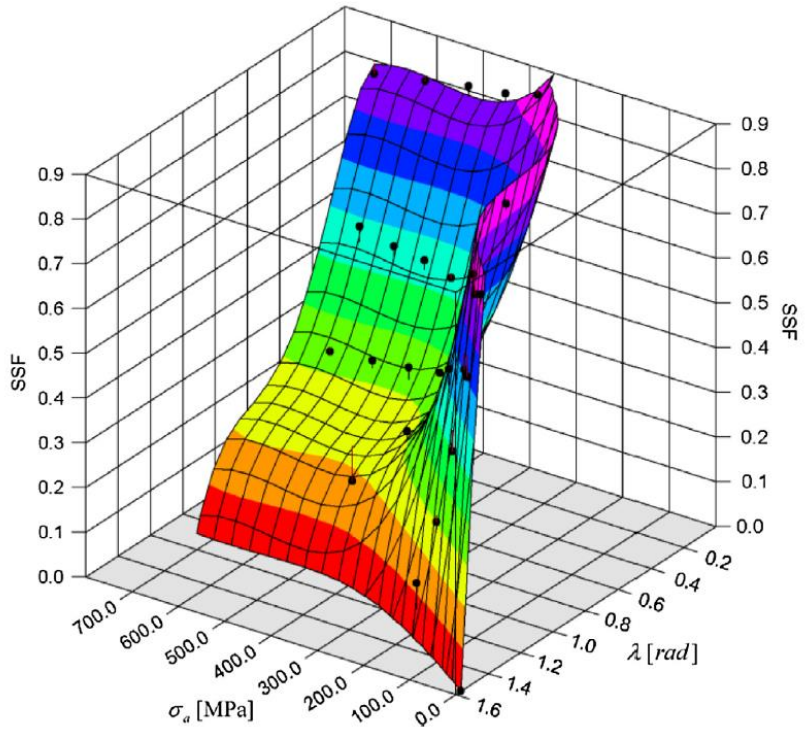

Figure 3.6 SSF surface[33].

The SSF surface presented in Figure 3.6 demonstrates how the damage scale varies with normal stress amplitude and stress amplitude ratio. This SSF surface was obtained using the five loading paths shown in Figure 3.1 for different stress amplitudes evaluated on the plane oriented at 0°.

From experiments it was observed that crack initiation planes are oriented according to the loading type, for instance, Figure 3.7 demonstrates the fracture surface for 42CrMo4 at proportional loading condition. The steel specimen fracture surface shows one crack origin and three distinct zones: the usual FZ and IZ zones and a surface wear region. The crack initiation plane angle measured for the steel specimen was -16 [23], which is a plane different from the one in which the SSF damage map is evaluated, plane oriented at 0°.

The -16° shown in figure 3.7 (c) represents the critical plane obtained from experimental results and this will be used to compute the SSF surface at this orientation so that it can be compared with the surface that was obtained at 0° (see Figure 3.6).

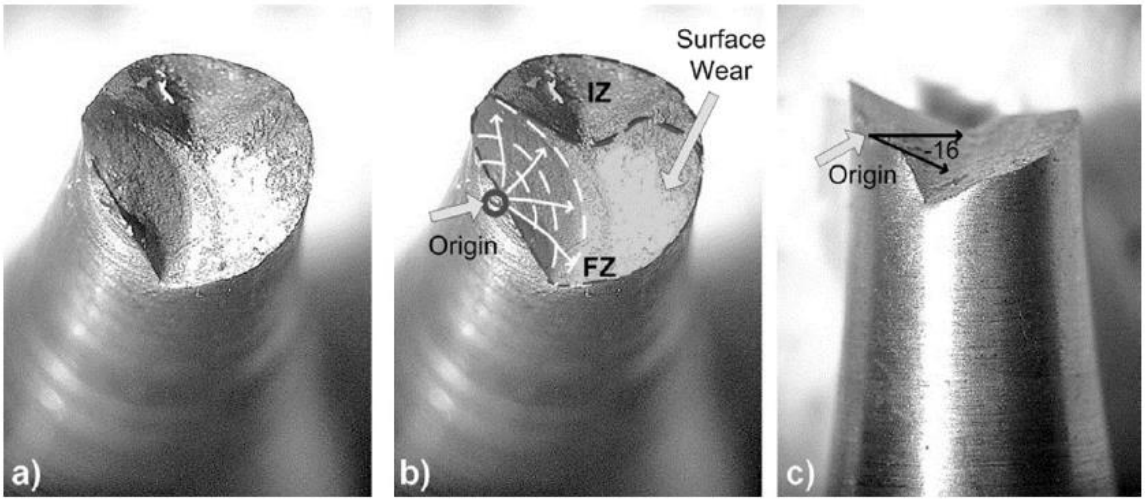

Figure 3.7 Shows the fracture surface (a and b) and the orientation of crack initiation (c)[23].

Table 3.8 shows the SSF data obtained for the case 4 loading cases shown in Figure 3.1(excepting the PS loading). These that will be used to perform regression from Datafit to obtain the SSF damage map at -16°. From Table 3.8, the first column contains the maximum normal stress amplitude for each loading phase and in the following column the stress amplitude ration is shown and finally the last column the calculated SSF for each loading case is shown.

Table 3.8 Experimental data used to obtain the SSF surface evaluated at -16°.

σ_a(MPa)	λ(rad)	SSF
636	0	0.61
555	0	0.60
484	0	0.60
423	0	0.59
370	0	0.59
490	0.32	0.42
435	0.32	0.40
386	0.32	0.38
342	0.32	0.35
304	0.32	0.34
402	0.52	0.19
344	0.52	0.21
297	0.52	0.22
255	0.52	0.24
219	0.52	0.26
200	0.79	0.01
153	0.79	0.39
117	0.79	0.82
90	0.79	1.32
69	0.79	1.87
0	1.57	0
0	1.57	0
0	1.57	0
0	1.57	0
0	1.57	0

Based on the experimental data, Eq. (3.2) was obtained with the goodness of fit being $R^2 = 0.998$, this result means good regression estimates that fits very well the experimental data, this is because $R^2 = 1$ means that the predicted values fully fit on the experimental ones. The regression variable results are shown in Table 3.9.

Table 3.9 Damage map variables obtained by regression using Datafit.

Variable	Value
a	5.377203261
b	-5.57E-02
c	2.50E-04
d	-5.49E-07
e	5.91E-10
f	-2.51E-13
g	-0.446710686
h	-0.970413066
i	1.677887313
j	-1.44462275

$$SSF(\sigma_a, \lambda) = a + b\sigma_a + c\sigma_a^2 + d\sigma_a^3 + e\sigma_a^4 + f\sigma_a^5 + g\lambda + h\lambda^2 + i\lambda^3 + j\lambda^4 \qquad (3.2)$$

Figure 3.8 shows the SSF damage map evaluated at the critical plane orientation (-16°). It can also be observed that the evolution of the SSF surface at -16° is less complicated than the SSF surface evaluated at 0°. This difference in the SSF surface geometry shows that the SSF can be computed in other orientations with surfaces that behaves better than the one obtained at 0°, this means that there are orientations that make easier to perform the fitting and hence minimising the error.

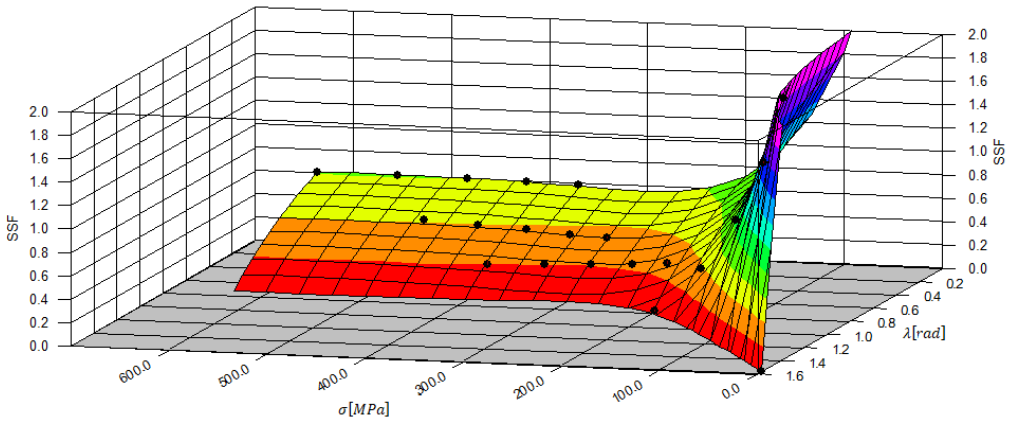

Figure 3.8 SSF surface for the critical plane orientation (-16).

This analysis was extended by plotting SSF surface for others plane directions in order to observe the behaviour of SSF surface for those orientations. For this study it was only plotted

SSF surface for -5, -10, -15 and -20 which are orientations around the critical plane angle(-16°) and the orientation where SSF parameter was evaluated (0°). In Figure 3.9 the SSF surface for -5°, -10°, -15° and -20° is shown and R^2 value for each case is presented in Table 3.10.

Table 3.10 The R^2 for each plane orientation.

Plane direction	R square
-5°	0.994
-10°	0.996
-15°	0.997
-20°	0.998

The SSF surfaces shown in Figure 3.9 demonstrates that as the plane orientations decreases the surface becomes less curved. For instance, it can be observed that Figure 3.9 (a) SSF surface is much curved than others surfaces (b, c and d) and as R^2 becomes bigger the SSF surface become less complicated. From these figures it can be concluded that there may be other orientation which the error can still be further reduced. These figures also confirmed that the damage map changes with plane direction.

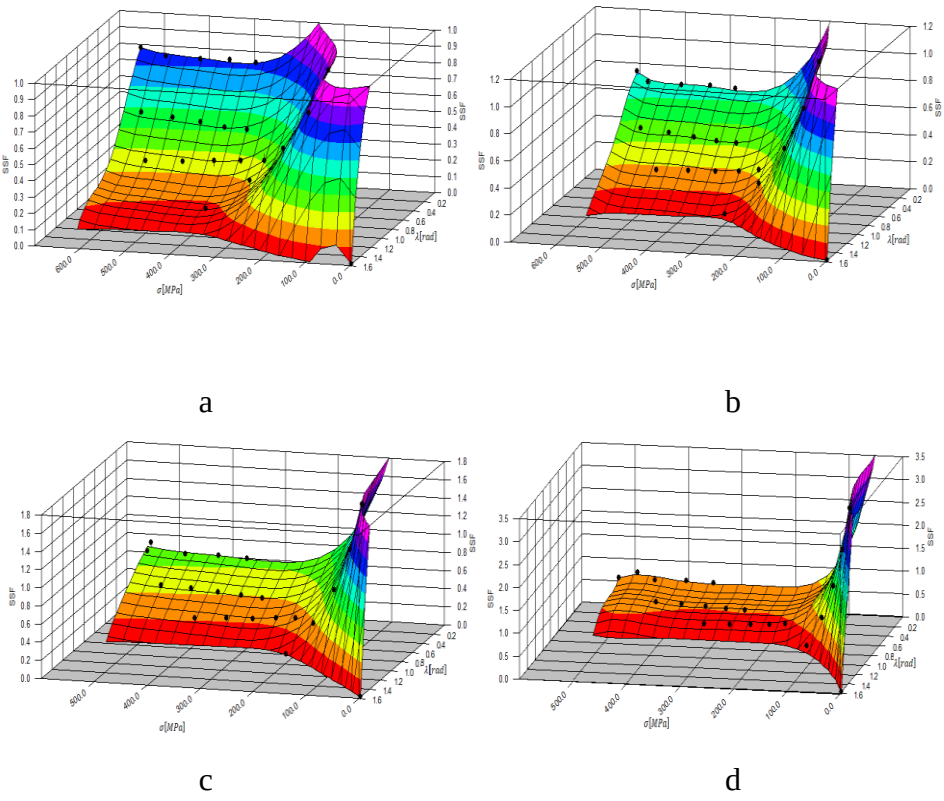

a b c d

Figure 3.9 SSF surface for four different plane orientations: (a) -5; (b) -10; (c) -15 and (d) -20.

In order to determine the correlation that exists between experimental fatigue life and estimated fatigue life a uniaxial shear trend line was considered (see Annex A.2). The crack path amplitude as well as experimental fatigue results for the critical plane angle are presented in Table 3.11. With the crack path amplitudes, the shear and normal stress corresponding to the critical plane orientation (-16°) were obtained using Eq.(s) 2.6 and 2.7.

Table 3.11 Experimental fatigue life for 42CrMo4 [23].

Loading case	Normal stress (MPa)	Shear stress (MPa)	N_f
PP	425	245.4	1000000 (run out)
PP	600	251.1	564088
PP	560	254.0	311401
PP	550	256.9	239600
PP	495	268.5	109087
PP	485	271.4	97366
PP	480	285.8	48740
PP	520.0	300.2	27204
PP	610.0	352.2	4114

From Figure 3.10 the correlation between experimental fatigue life and estimated fatigue life is presented and fatigue life factor of 3 was used. From figure 3.10, it is possible to see that all the results are within the fatigue life factor boundary. From the results most points are above the reference line with only one being below the reference and other nearly reached the middle line this means that the results are nonconservative.

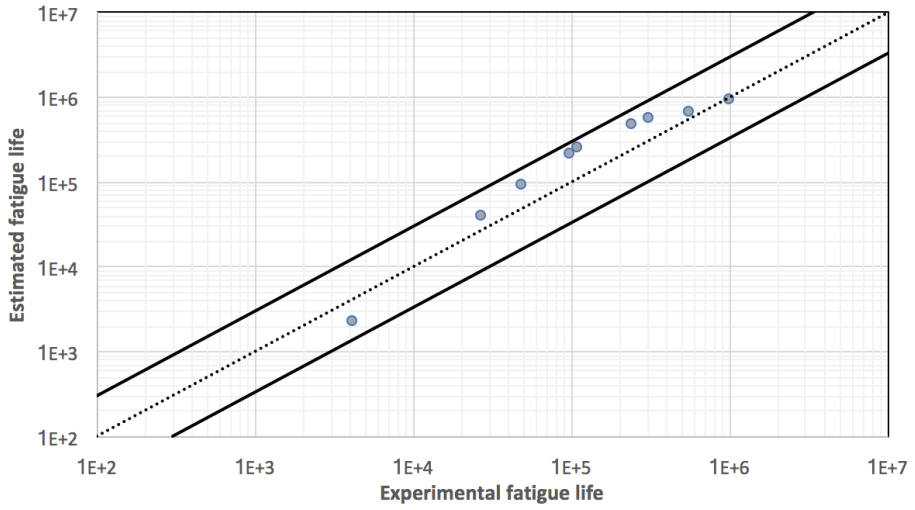

Figure 3.10 Correlation between estimated and experimental fatigue life.

Therefore, the fatigue life results obtained in this study shows that using the damage scale at -16 degrees, it is possible to estimate good fatigue life results in this particular plane.

3.4 Critical plane results

To obtain the damage parameter and their corresponding plane orientation the formulas described in section 2.4 were used. With the formulation of each of the critical plane model discussed in section 2.4, a damage parameter was obtained for each plane orientation starting from -90° to 90°. The critical plane is identified as the plane that experiences the most damage. In this study it was considered four critical plane models such as SWT, Brown-Miller, Fatemi-Socie and Liu (which is Liu I +Liu II) in each case the normal stress considered was 435MPa.

In Fig.(s) 3.11 to 3.14 the damage parameter evolution with the plane orientation is demonstrated. By observing figure each figure the critical plane angle can be clearly observed.

SWT

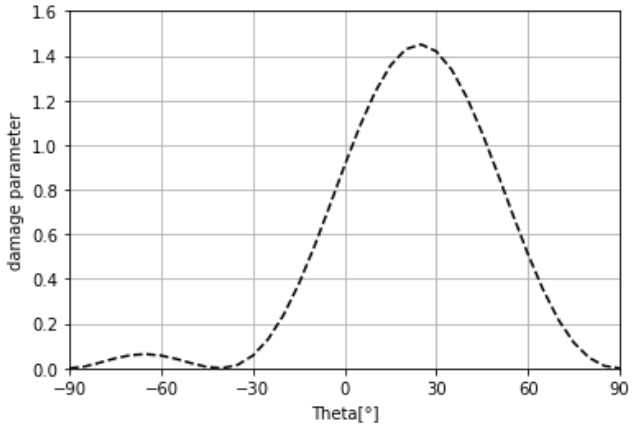

Figure 3.11 Critical plane estimation for SWT damage parameter.

Brown-Miller

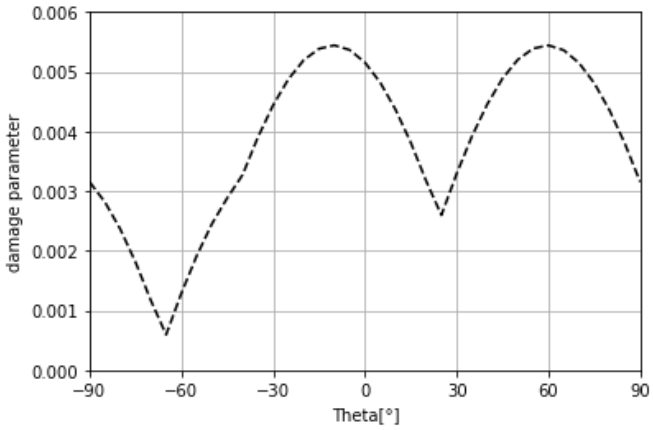

Figure 3.12 Critical plane estimation Brown-Miller damage parameter.

Fatemi-Socie

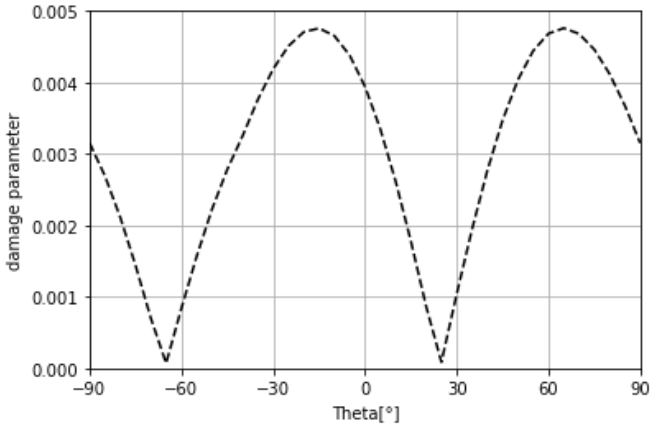

Figure 3.13 Critical plane estimation for Fatemi-Socie damage parameter.

Liu

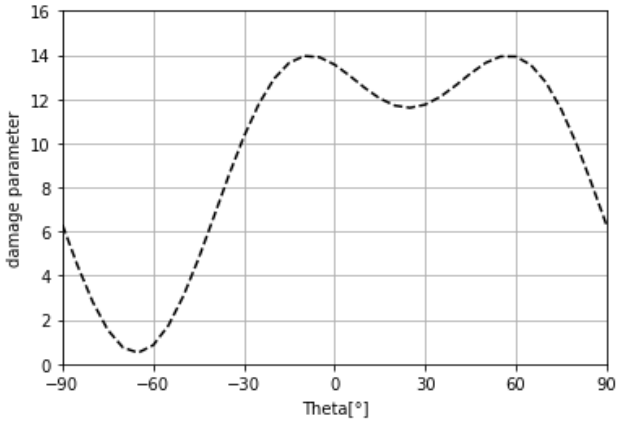

Figure 3.14 Critical plane estimation for Liu damage parameter.

Looking at the estimated critical plane angles compared to experimental results (-16°), from Table 3.6 it can be seen that for SWT the critical plane angle is 25° which means that this approach predicts a poor result. However, this is expected because the SWT works better for material that fail under maximum tensile stress or strain.

As can be also seen from Table 3.12, Brown-Miller, Fatemi-Socie and Liu predicted well the critical plane angle. For damage parameters which crack initiation is dominated by shear stress (Fatemi-Socie and Brown Miller) these results are expected due to the fact that 42CrMo4 is considered as ductile material which the dominant failure mechanics is nucleation and crack growth due to shearing. Amongst all the critical plane models the Fatemi- Socie approach predicted better result.

Table 3.12 Comparison between estimated and measured critical plane for 42CrMo4.

Critical Plane models	Angle
Measured	-16°
SWT	25°
Brown-Miller	-10°,60°
Fatemi-Socie	-15°,65°
Liu	-10, 60°

3.5 Alternative approach to determine damage surface map

In this section, an alternative approach to determine SSF damage surface map will be presented. The advantage of using this approach is that it does not require the use of Datafit, which is a paid software.

In order to determine the damage map using the proposed method only a Microsoft Excel knowledge is required. It is known that the SSF damage parameter depends both on stress amplitude and stress amplitude ratio, this means in this alternative approach these parameters must be considered. The aim of this approach is to model SSF with a third order polynomial, see Eq. (3.3).

$$SSF = Ax^3 + Bx^2 + Cx + D \tag{3.3}$$

From Eq. (3.3), $x = \sigma$ and A, B, C and D are constants that are dependent on the stress amplitude ratio.

To begin with, the SSF variation with stress amplitude for all the loading paths is plotted in a single graph, as shown in Figure 3.15. For each loading path, a third order polynomial is obtained together with the corresponding coefficient of determination, R^2. For this particular case, all the third order polynomial have an error very close to 1, which means that it is a good approximation.

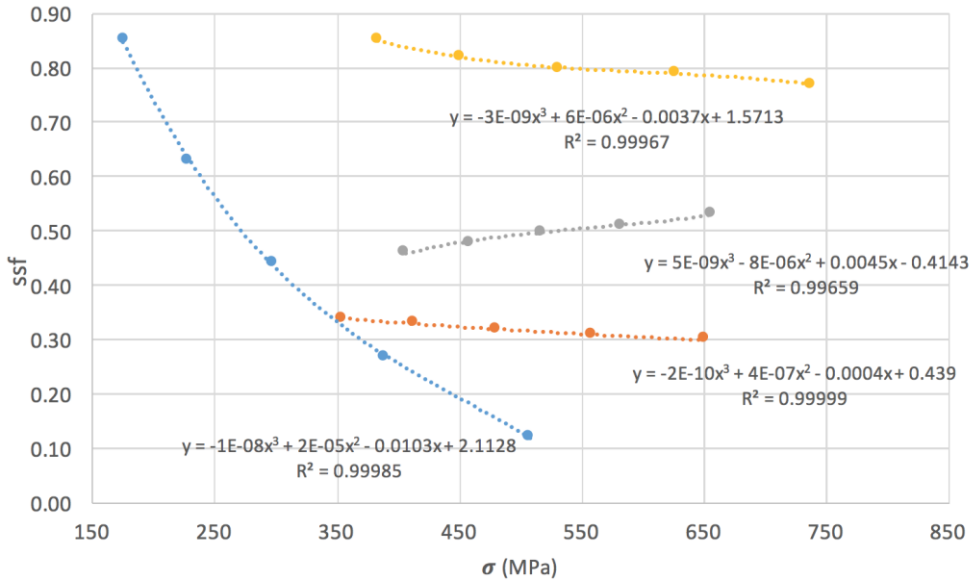

Figure 3.15 SSF evolution with stress amplitude for four different loading paths at the critical plane orientation (-16°).

The third order polynomial that is obtained for each of the loading have four constants associated with it. From Figures 3.15, each polynomial represents one loading path and one stress amplitude ratio. Since there are four loading paths, the SAR representing each of the loading and their corresponding constants are presented in Table 3.13.

Table 3.13 Stress amplitude ratio and constants associated with the third order polynomial for each loading path.

λ	a	b	c	d
0	-5.00E-10	7.00E-07	-0.0003	0.6213
0.32	5.00E-09	-6.00E-06	0.0016	0.4453
0.52	-7.00E-09	7.00E-06	-0.0030	0.6255
0.79	-6.00E-07	3.00E-04	-0.0667	5.1102

The stress amplitude ratio presented in Table 3.9 is plotted against each of the constants see figure 3.16 a) to d). This is done in a way that constants A, B, C and D can be represented as a function of stress amplitude ratio. From figure 3.16, a third polynomial and coefficient of determination is obtained for each constant and using these graphs the value of each constant can be estimated as long as stress amplitude ratio is known.

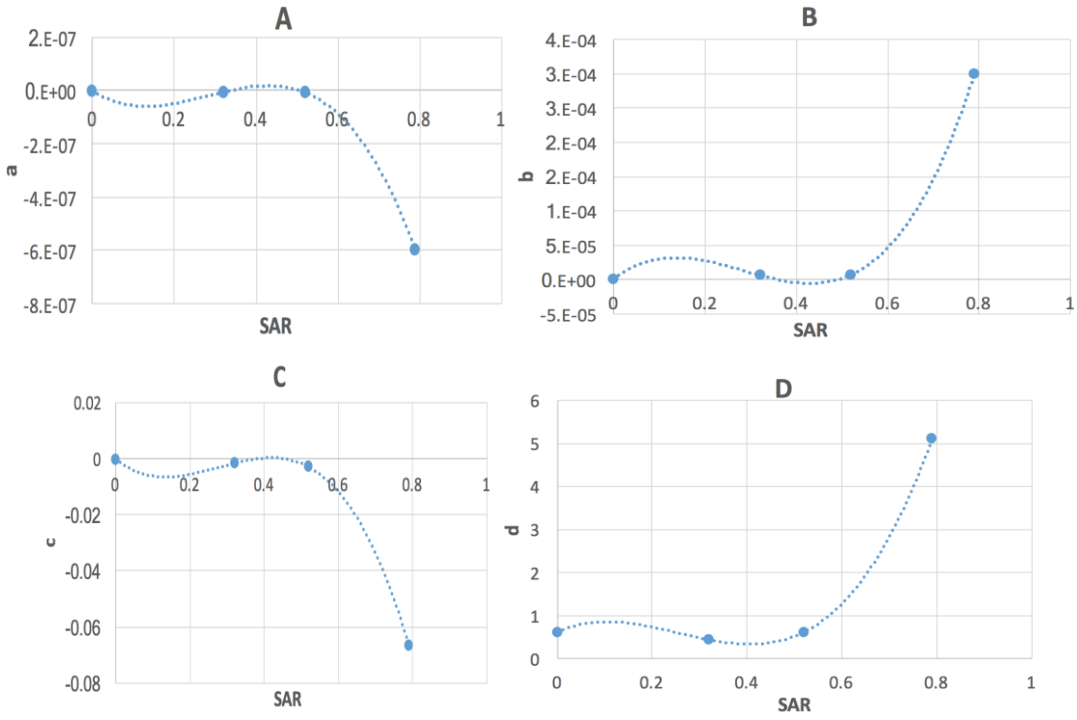

Figure 3.16 Stress amplitude ratio variation with constants.

The third order polynomial for each constant is presented below, see equation 3.4 to 3.7. In each case the $R^2 = 1$, this means that there is no error associated with these approximations.

$$A = -5.9E10\lambda^3 + 4.96E - 09\lambda^2 - 9.98E - 09\lambda - 5E - 10 \quad (3.4)$$

$$B = 0.0029\lambda^3 - 0.0025\lambda^2 + 0.0005\lambda + 7E - 06 \quad (3.5)$$

$$C = -0.6094\lambda^3 + 0.5062\lambda^2 - 0.103659\lambda - 0.0003 \quad (3.6)$$

$$D = 36.018\lambda^3 - 25.285\lambda^2 + 2.72\lambda + 0.9839 \quad (3.7)$$

The Eq. (3.8) can be written in terms of stress amplitude and in terms of four constants that depends on the stress amplitude ratio.

$$SSF = A\sigma^3 + B\sigma^2 + C\sigma + D \quad (3.8)$$

In order to obtain damage surface map, the following strategy was considered:

1. Create a matrix from Microsoft Excel.

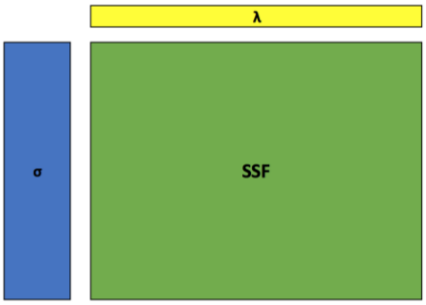

2. From Table 3.3, the maximum and minimum value of stress amplitude were considered. Starting from the minimum value a constant variation was considered until it reached the maximum value.
3. Again from Table 3.3, the maximum and minimum value of stress amplitude ratio were considered. From minimum value to maximum a variation of 0.2 was considered.
4. For each stress amplitude ratio, a value of constants A, B, C and D were calculated.
5. Once the constants were all known, equation 3.8 could be applied to calculate the SSF variation as the stress amplitude and stress amplitude ratio vary.

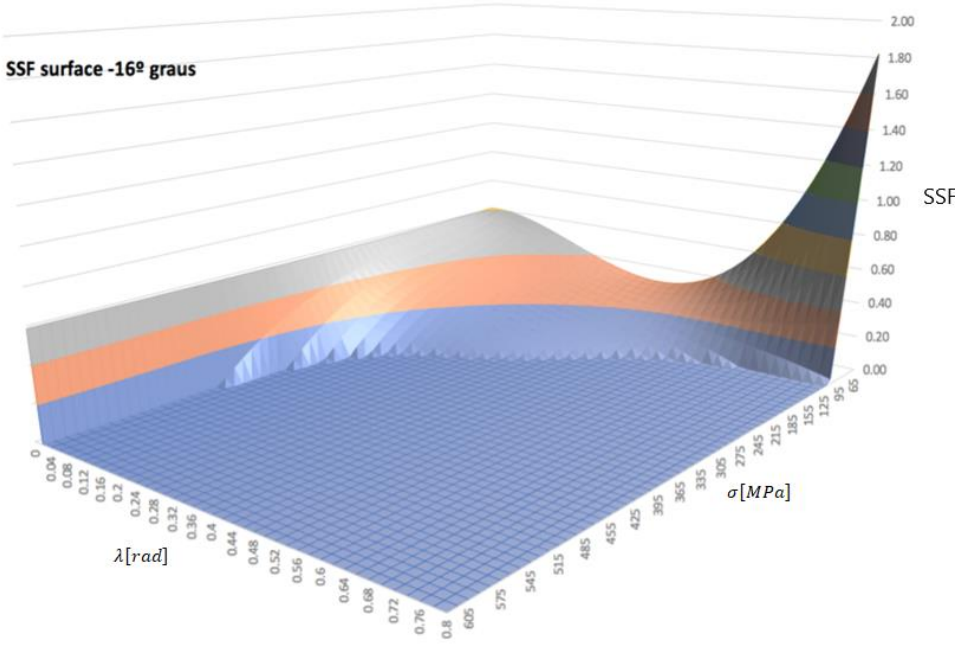

Figure 3.17 SSF surface for -16° using Excel approach.

It can be clearly observed that the SSF surface that was obtained using proposed approach (see Figure 3.17) have some differences in evolution when compared to the one

obtained using Datafit (see Figure 3.8). In both figures, it is possible to see that the SSF value decreased as stress amplitude increases which is expected to happen, however for Figure 3.17 the SSF value goes to negative for large part of the figure which means the SSF surface evolution do not follow fatigue physical phenomenon. The reason behind this may be because for 0° case the SSF surface is obtained considering a pure shear SN curve which is evaluated at 0° with the proportional loading at 0°, both curves are evaluated at the same plane. This is why at 0° both for Datafit and Excel the damage surface evolution looks similar with some small differences. However, for a -16° case we are still considering the uniaxial SN curve which remains at 0° while we are also evaluating the components of SN curve at – 16°. For a critical plane orientation, we are connecting the damage at 0° with the damage at -16°.

For now, it is not possible to apply this method directly, but we would have to evaluate the uniaxial shear SN curve for -16 degree first. Evaluating the SN curve at -16° will increase the complexity of the study so because of that we will focus our analysis again on 0°.

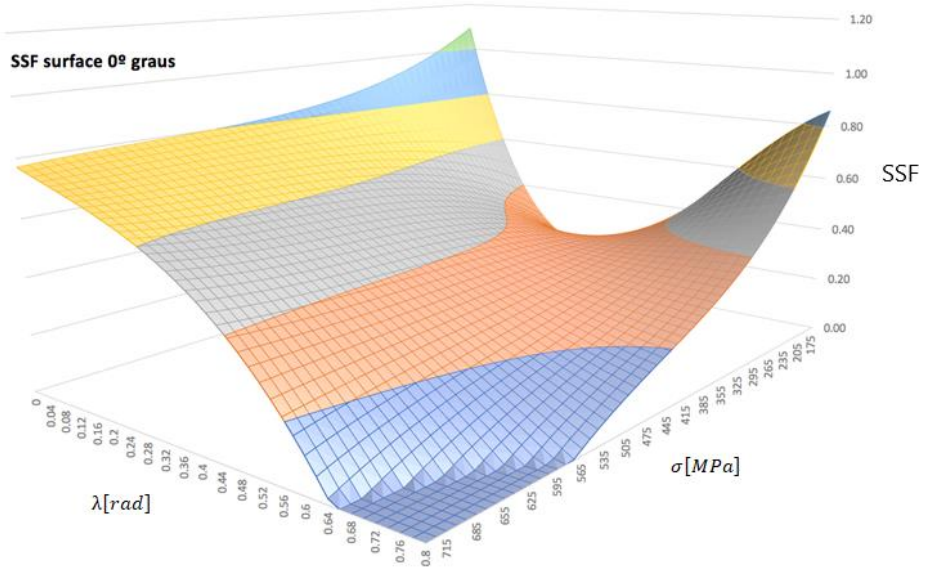

Figure 3.18 SSF surface for 0° using Excel approach.

$\lambda[rad]$

Moving the study to different plane orientation, the SSF surface obtained using Datafit will be compared with the one obtained using the proposed approach. The SSF surface obtained using Datafit at 0° is presented in Figure 3.6 and in Figure 3.18 the SSF surface obtained using the proposed methodology at the same plane orientation is shown.

Looking at both figure 3.6 and 3.18, it is possible to see that the surface that was obtained using Excel it is slightly less curved than the one obtained using Datafit. One key aspect to highlighted is that for Figure 3.18 the SSF values for certain range of stress amplitude and stress amplitude ratio becomes negative and this does not correspond to the fatigue physical phenomenon.

Table 3.14 Experimental fatigue life for 42CrMo4 [23].

Loading case	Normal stress (MPa)	Shear stress (MPa)	N_f
PT	700	0	6040
PT	600	0	19951
PT	560	0	53752
PT	550	0	56929
PT	495	0	247953
PT	485	0	269178
PT	480	0	1000000 (run out)

In figure 3.19 It is shown the comparison between estimated fatigue life and experimental fatigue life for 42CrMo4 evaluated at 0°. It can be seen that most of the experimental and estimated fatigue life results are within the boundary which has a fatigue life factor of 3. It is also important to mention that fatigue life results obtained using Datafit has more fatigue life results above the reference line, which means that these results are nonconservative. A nonconservative results means that under proportional loading the value of the SSF equivalent stress is lower than it should be.

It can also be observed from Figure 3.19 that the fatigue life results obtained using the proposed approach have more results on the reference line than the fatigue life results obtained using Datafit. This means that the proposed approach yields to better fatigue life results than Datafit.

The fatigue life results shown in Figure 3.19 demonstrates that there may exist another function outside Datafit database that can be used to model SSF and even predict better results. From figure 3.19, it can also be concluded that using the proposed approach it is possible to obtain good fatigue life results. That said, instead of using a paid software to determine the damage map a similar or better estimation can be achieved using the alternative approach which only requires good excel knowledge.

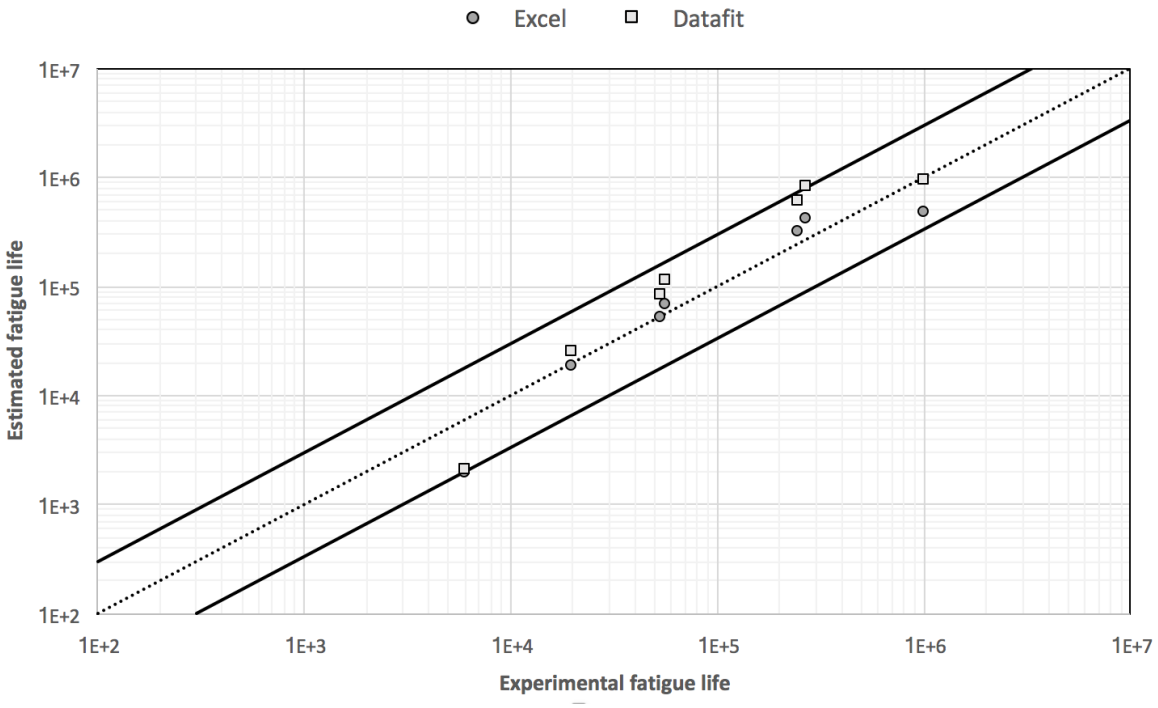

Figure 3.19 Comparison between experimental fatigue and estimated fatigue that was obtained using Datafit and excel approach.

4. Conclusion and future works

In this dissertation it was done a literature review concerning the multiaxial fatigue. The review started from basic fatigue knowledge, plane models, cycle counting methods to the most used damage accumulation method, Miner's Rule. From the literature review the stress scale factor (SSF) approach was explore and from the stress scale factor approach several analyses were done. By analysing the results in chapter 3, several conclusions can be drawn:

- Using the methodology to assess the SSF damage map it was proved that the SSF in fact varies with the plane orientation. This variation helps to understand the main reason that makes the critical plane approach to generate poor fatigue life estimates.
- Concerning the plane in which the damage map is evaluated and using the experimental critical plane angle for the PP45 loading path at -16°, it was shown that there may be other plane orientations in which the damage surface can be computed with improved fatigue life estimates comparatively to the results obtained at 0°.
- Using the proposed approach (Excel based approach) to determine the SSF damage at 0°, it was possible to obtain good agreements with experimental data. Furthermore, with the proposed approach a better fatigue life estimates have been obtained which means once the proposed approach is fully validated it can be used instead of Datafit.

It was seen that SSF damage map obtained using the proposed approach at -16° resulted in some SSF results being negative, which do not correspond to the fatigue failure phenomenon. Therefore, in order to overcome this, the uniaxial 0° SN curve should be evaluated at -16°. Having the SN curve evaluated at -16° will allow us to connect the uniaxial SN curve together with the proportional loading to evaluate the damage scale between normal and shear stresses at the same plane. By doing this, there will be two SSF, one for normal component and the other for the shear component. This means that the reference shear component of the uniaxial loading can be compared to the shear component projected at -16° and it is also possible to compare the normal component that results from the uniaxial projection at -16° with the loading for -16°. The fact that there will be two SSF means that there will also be two SSF surfaces.

One other thing that can be considered to improve the results obtained using the proposed approach is changing the degree of polynomial that describes the SSF evolution, this should be done in the future because those curves shown in Figure 3.13 may not be the real representation of fatigue physical phenomenon, perhaps considering polynomial of higher order could improve the SSF surface at -16° and thus predicting improved fatigue life.

Once the Excel method is validated it will facilitate the automation of this method. All of this methodology/algorithm can be passed into an Excel, Python or Matlab script. Having this approach automated will make it quicker to obtain the damage surface for several orientations and in short period of time it can be determined which plane has the highest or lowest damage.

Since the SSF approach does not take into consideration the mean stress effect, it would be needed in the future to study how mean stress could affect the damage scale.

References

[1] N. E. Dowling, K. Siva Prasad, and R. Narayanasamy, *Mechanical behavior of materials: engineering methods for deformation, fracture, and fatigue*, 4. ed., Internat. ed. Boston, Mass.: Pearson, 2013.

[2] S. H. Baek, J. H. Jeon, K. Y. Lee, S. S. Cho, and W. S. Joo, 'Reliability Analysis and Preventive Maintenance for Fatigue Life of End Beam for Uncovered Freight Car', *Transactions of the Korean Society of Mechanical Engineers A*, vol. 29, no. 3, pp. 495–502, Mar. 2005, doi: 10.3795/KSME-A.2005.29.3.495.

[3] S. H. Baek, S. S. Cho, and W. S. Joo, 'Fatigue life prediction based on the rainflow cycle counting method for the end beam of a freight car bogie', *Int.J Automot. Technol.*, vol. 9, no. 1, pp. 95–101, Feb. 2008, doi: 10.1007/s12239-008-0012-y.

[4] W. D. Callister and W. D. Callister, *Fundamentals of materials science and engineering: an interactive etext*. New York: Wiley, 2001.

[5] R. P. Reed, J. H. Smith, and B. W. Christ, 'Economic effects of fracture in the United States. Part 1. A synopsis of the September 30, 1982 report to NBS by Battelle Columbus Laboratories', United States, 1983.

[6] H. P. Rossmanith, 'George Rankin Irwin-The Father of Fracture Mechanics 1907-1998', *Fragblast*, vol. 2, no. 2, pp. 123–141, Jan. 1998, doi: 10.1080/13855149809408882.

[7] I. Milne, 'The importance of the management of structural integrity', *Engineering Failure Analysis*, vol. 1, no. 3, pp. 171–181, Oct. 1994, doi: 10.1016/1350-6307(94)90016-7.

[8] I. Milne, B. Karihaloo, and R. O. Ritchie, 'Structural Integrity Assurance', in *Comprehensive Structural Integrity*, Elsevier, 2003, pp. 1–24. doi: 10.1016/B0-08-043749-4/01077-6.

[9] 'Fatigue Properties in Engineering', in *Fatigue and Fracture*, ASM International, 1996, pp. 15–26. doi: 10.31399/asm.hb.v19.a0002350.

[10] R. A. Smith and S. Hillmansen, 'A brief historical overview of the fatigue of railway axles', *Proceedings of the Institution of Mechanical Engineers, Part F: Journal of Rail and Rapid Transit*, vol. 218, no. 4, pp. 267–277, Jul. 2004, doi: 10.1243/0954409043125932.

[11] R. A. Smith, 'Fatigue of railway axles: A classic problem revisited', in *European Structural Integrity Society*, vol. 26, Elsevier, 2000, pp. 173–181. doi: 10.1016/S1566-1369(00)80049-7.

[12] S. Timoshenko, *History of strength of materials: with a brief account of the history of theory of elasticity and theory of structures*. New York: Dover Publications, 1983.

[13] J. Ewing and J. Humfrey, 'VI. The fracture of metals under repeated alternations of stress', *Phil. Trans. R. Soc. Lond. A*, vol. 200, no. 321–330, pp. 241–250, Jan. 1903, doi: 10.1098/rsta.1903.0006.

[14] O. H. Basquin, 'The exponential law of endurance tests.', *American Society for Testing Materials*, vol. 10, pp. 625–630, 1910.

[15] S. S. Manson, 'Discussion: "Experimental Support for Generalized Equation Predicting Low Cycle Fatigue" (Tavernelli, J. F., and Coffin, Jr., L. F., 1962, ASME J. Basic Eng., 84, pp. 533–537)', *Journal of Basic Engineering*, vol. 84, no. 4, pp. 537–541, Dec. 1962, doi: 10.1115/1.3658702.

[16] A. Fatemi and N. Shamsaei, 'Multiaxial fatigue: An overview and some approximation models for life estimation', *International Journal of Fatigue*, vol. 33, no. 8, pp. 948–958, Aug. 2011, doi: 10.1016/j.ijfatigue.2011.01.003.

[17] H. Zenner, ‘Multiaxial fatigue – methods, hypotheses and applications: This keynote has been published also in the Proceedings of the 7th International Conference on Biaxial/Multiaxial Fatigue and Fracture (7th ICBMFF)’, *MP*, vol. 47, no. 5, pp. 249–254, May 2005, doi: 10.3139/120.100655.
[18] Y.-L. Lee, Ed., *Fatigue testing and analysis: theory and practice*. Amsterdam ; Boston: Elsevier Butterworth-Heinemann, 2005.
[19] J. Schijve, *Fatigue of structures and materials*, Second edition. Dordrecht: Springer, 2009.
[20] N. E. Dowling, ‘Mean Stress Effects in Stress-Life and Strain-Life Fatigue’, Apr. 2004, pp. 2004-01–2227. doi: 10.4271/2004-01-2227.
[21] L. Silva, *Comportamento Mecânico dos Materiais*. Porto: PUBLINDUSTRIA, 2012.
[22] Macha and Sonsino, ‘Energy criteria of multiaxial fatigue failure’, *Fat Frac Eng Mat Struct*, vol. 22, no. 12, pp. 1053–1070, Dec. 1999, doi: 10.1046/j.1460-2695.1999.00220.x.
[23] V. Anes, L. Reis, B. Li, and M. Freitas, ‘Crack path evaluation on HC and BCC microstructures under multiaxial cyclic loading’, *International Journal of Fatigue*, p. 12, 2014.
[24] D. Socie and G. Marquis, *Multiaxial fatigue*. Warrendale, Pa: Society of Automotive Engineers, 2000.
[25] M. W. Brown and K. J. Miller, ‘A Theory for Fatigue Failure under Multiaxial Stress-Strain Conditions’, *Proceedings of the Institution of Mechanical Engineers*, vol. 187, no. 1, pp. 745–755, Jun. 1973, doi: 10.1243/PIME_PROC_1973_187_069_02.
[26] K. Lieb *et al.*, ‘Multiaxial Fatigue: A Survey of the State of the Art’, *J. Test. Eval.*, vol. 9, no. 3, p. 165, 1981, doi: 10.1520/JTE11553J.
[27] S. Y. Zamrik and R. E. Frishmuth, ‘The effects of out-of-phase biaxial-strain cycling on low-cycle fatigue: Experimental investigation shows a particular phase effect on crack growth and failure mode in the selected low-cycle-fatigue range’, *Experimental Mechanics*, vol. 13, no. 5, pp. 204–208, May 1973, doi: 10.1007/BF02322654.
[28] A. Fatemi and D. F. Socie, ‘A CRITICAL PLANE APPROACH TO MULTIAXIAL FATIGUE DAMAGE INCLUDING OUT-OF-PHASE LOADING’, *Fat Frac Eng Mat Struct*, vol. 11, no. 3, pp. 149–165, Mar. 1988, doi: 10.1111/j.1460-2695.1988.tb01169.x.
[29] R. I. Stephens and H. O. Fuchs, Eds., *Metal fatigue in engineering*, 2nd ed. New York: Wiley, 2001.
[30] D. F. Socie and T. W. Shield, ‘Mean Stress Effects in Biaxial Fatigue of Inconel 718’, *Journal of Engineering Materials and Technology*, vol. 106, no. 3, pp. 227–232, Jul. 1984, doi: 10.1115/1.3225707.
[31] R. N. Smith, P. Watson, and T. H. Topper, ‘A Stress-Strain Parameter for Fatigue Metals.’, *Journal of Materials*, vol. 5, pp. 767–778, 1970.
[32] K. Liu, ‘A Method Based on Virtual Strain-Energy Parameters for Multiaxial Fatigue Life Prediction’, in *Advances in Multiaxial Fatigue*, D. McDowell and J. Ellis, Eds. 100 Barr Harbor Drive, PO Box C700, West Conshohocken, PA 19428-2959: ASTM International, 1993, pp. 67-67–18. doi: 10.1520/STP24796S.
[33] V. Anes, L. Reis, B. Li, M. Fonte, and M. de Freitas, ‘New approach for analysis of complex multiaxial loading paths’, *International Journal of Fatigue*, vol. 62, pp. 21–33, May 2014, doi: 10.1016/j.ijfatigue.2013.05.004.
[34] L. Reis, B. Li, and M. De Freitas, ‘Analytical and experimental studies on fatigue crack path under complex multi-axial loading’, *Fat Frac Eng Mat Struct*, vol. 29, no. 4, pp. 281–289, Apr. 2006, doi: 10.1111/j.1460-2695.2006.01001.x.

[35] L. Reis, V. Anes, B. Li, and M. de Freitas, ‘Damage Accumulation Due to Sequential Loading Effect’, *Procedia Engineering*, vol. 10, pp. 1396–1401, 2011, doi: 10.1016/j.proeng.2011.04.232.
[36] V. Anes, L. Reis, and M. de Freitas, ‘On the assessment of multiaxial fatigue damage under variable amplitude loading’, *Frattura ed Integrità Strutturale*, vol. 10, no. 37, pp. 124–130, Jun. 2016, doi: 10.3221/IGF-ESIS.37.17.
[37] E08 Committee, ‘Practices for Cycle Counting in Fatigue Analysis’, ASTM International. doi: 10.1520/E1049-85R05.
[38] Matsuishi and T. Endo, ‘Fatigue of metals subjected to varying stress’, *Japan Society of Mechanical Engineering*, 1968.
[39] Y.-L. Lee, M. E. Barkey, and H.-T. Kang, *Metal fatigue analysis handbook: practical problem-solving techniques for computer-aided engineering*. Waltham, MA: Butterworth-Heinemann, 2012.
[40] S. Downing and D. Socie, ‘Simple rainflow counting algorithms’, *International Journal of Fatigue*, vol. 4, no. 1, pp. 31–40, Jan. 1982, doi: 10.1016/0142-1123(82)90018-4.
[41] J. A. Bannantine, J. J. Comer, and J. L. Handrock, *Fundamentals of metal fatigue analysis*. Englewood Cliffs, N.J: Prentice Hall, 1990.
[42] C. Amzallag, J. Gerey, J. Robert, and J. Bahuaud, ‘Standardization of the rainflow counting method for fatigue analysis’, *International Journal of Fatigue*, vol. 16, no. 4, pp. 287–293, Jun. 1994, doi: 10.1016/0142-1123(94)90343-3.
[43] C. H. McInnes and P. A. Meehan, ‘Equivalence of four-point and three-point rainflow cycle counting algorithms’, *International Journal of Fatigue*, vol. 30, no. 3, pp. 547–559, Mar. 2008, doi: 10.1016/j.ijfatigue.2007.03.006.
[44] M. A. Meggiolaro and J. T. P. de Castro, ‘An improved multiaxial rainflow algorithm for non-proportional stress or strain histories – Part I: Enclosing surface methods’, *International Journal of Fatigue*, vol. 42, pp. 217–226, Sep. 2012, doi: 10.1016/j.ijfatigue.2011.10.014.
[45] M. Azamfar and M. Moshrefifar, ‘Moshrefifar and Azamfar method, a new cycle counting method for evaluating fatigue life’, *International Journal of Fatigue*, vol. 69, pp. 2–15, Dec. 2014, doi: 10.1016/j.ijfatigue.2014.03.020.
[46] T. Langlais, ‘Multiaxial cycle counting for critical plane methods’, *International Journal of Fatigue*, vol. 25, no. 7, pp. 641–647, Jul. 2003, doi: 10.1016/S0142-1123(02)00148-2.
[47] V. Anes, L. Reis, and M. Freitas, ‘Multiaxial Fatigue Damage Accumulation under Variable Amplitude Loading Conditions’, *Procedia Engineering*, vol. 101, pp. 117–125, 2015, doi: 10.1016/j.proeng.2015.02.016.
[48] J. Papuga, ‘Mapping of fatigue damages’, Program Shell of FE-Calculation, CTU, Prague, 2005.
[49] N. Shamsaei, A. Fatemi, and D. F. Socie, ‘Multiaxial fatigue evaluation using discriminating strain paths’, *International Journal of Fatigue*, vol. 33, no. 4, pp. 597–609, Apr. 2011, doi: 10.1016/j.ijfatigue.2010.11.002.
[50] Z. Wei and P. Dong, ‘A generalized cycle counting criterion for arbitrary multi-axial fatigue loading conditions’, *The Journal of Strain Analysis for Engineering Design*, vol. 49, no. 5, pp. 325–341, Jul. 2014, doi: 10.1177/0309324713515465.
[51] C. H. Wang and M. W. Brown, ‘Life Prediction Techniques for Variable Amplitude Multiaxial Fatigue—Part 1: Theories’, *Journal of Engineering Materials and Technology*, vol. 118, no. 3, pp. 367–370, Jul. 1996, doi: 10.1115/1.2806821.
[52] M. A. Meggiolaro and J. T. P. de Castro, ‘An improved multiaxial rainflow algorithm for non-proportional stress or strain histories – Part II: The Modified Wang–Brown

method', *International Journal of Fatigue*, vol. 42, pp. 194–206, Sep. 2012, doi: 10.1016/j.ijfatigue.2011.10.012.
[53] C. H. Wang and M. W. Brown, 'Life Prediction Techniques for Variable Amplitude Multiaxial Fatigue—Part 2: Comparison With Experimental Results', *Journal of Engineering Materials and Technology*, vol. 118, no. 3, pp. 371–374, Jul. 1996, doi: 10.1115/1.2806822.
[54] M. Margetin and D. Biro, 'Performance of chosen multiaxial cycle counting method under non-proportional multiaxial variable loading.', *MATEC Web Conf.*, vol. 165, p. 16008, 2018, doi: 10.1051/matecconf/201816516008.
[55] V. Anes, L. Reis, B. Li, and M. de Freitas, 'New cycle counting method for multiaxial fatigue', *International Journal of Fatigue*, vol. 67, pp. 78–94, Oct. 2014, doi: 10.1016/j.ijfatigue.2014.02.010.
[56] P. Dong, Z. Wei, and J. K. Hong, 'A path-dependent cycle counting method for variable-amplitude multi-axial loading', *International Journal of Fatigue*, vol. 32, no. 4, pp. 720–734, Apr. 2010, doi: 10.1016/j.ijfatigue.2009.10.010.
[57] J. A. Bannantine and D. F. Socie, 'A variable amplitude multiaxial fatigue life prediction method.', Third International Conference on Biaxial/Multiaxial Fatigue, Stuttgard, Germany, 1989.
[58] W. Hwang and K. S. Han, 'Cumulative Damage Models and Multi-Stress Fatigue Life Prediction', *Journal of Composite Materials*, vol. 20, no. 2, pp. 125–153, Mar. 1986, doi: 10.1177/002199838602000202.
[59] M. A. Miner, 'Cumulative damage in fatigue', vol. 12, J Appl Mech, 1945, pp. 159–164.
[60] S. Schoenborn, H. Kaufmann, C. M. Sonsino, and R. Heim, 'Cumulative Damage of High-strength Cast Iron Alloys for Automotive Applications', *Procedia Engineering*, vol. 101, pp. 440–449, 2015, doi: 10.1016/j.proeng.2015.02.053.
[61] A. Fatemi and L. Yang, 'Cumulative fatigue damage and life prediction theories: a survey of the state of the art for homogeneous materials', *International Journal of Fatigue*, vol. 20, no. 1, pp. 9–34, Jan. 1998, doi: 10.1016/S0142-1123(97)00081-9.
[62] Y. Kondo, 'Fatigue Under Variable Amplitude Loading', in *Comprehensive Structural Integrity*, Elsevier, 2003, pp. 253–279. doi: 10.1016/B0-08-043749-4/04029-5.
[63] P. Johannesson, *Guide to load analysis for durability in vehicle engineering*. Chichester: Wiley, 2014.
[64] M. Musallam and C. M. Johnson, 'An Efficient Implementation of the Rainflow Counting Algorithm for Life Consumption Estimation', *IEEE Trans. Rel.*, vol. 61, no. 4, pp. 978–986, Dec. 2012, doi: 10.1109/TR.2012.2221040.
[65] W. J. Staszewski, C. Boller, and G. R. Tomlinson, Eds., *Health monitoring of aerospace structures: smart sensor technologies and signal processing*. West Sussex, England: Hoboken, NJ : J. Wiley, 2004.

Annexes

A.1 Stress scale factor (SSF) for pure normal and three proportional loading paths evaluated at 0°.

Case 1, values in (MPa).

N_f	$\overline{AC}$ Pure shear amplitude	$\overline{AB}$ Shear amplitude	$\overline{AD}$ Axial amplitude	$\overline{BC}$ Shear increment	ssf
1.E+03	567	0	737	0	0.77
1.E+04	493	0	626	0	0.79
1.E+05	428	0	532	0	0.81
1.E+06	372	0	452	0	0.82
1.E+07	324	0	383	0	0.84

Case 3, values in (MPa).

N_f	$\overline{AC}$ Pure shear amplitude	$\overline{AB}$ Shear amplitude	$\overline{AD}$ Axial amplitude	$\overline{BC}$ Shear increment	ssf
1.E+03	567	219	656	349	0.53
1.E+04	493	194	582	299	0.51
1.E+05	428	172	516	256	0.50
1.E+06	372	153	458	220	0.48
1.E+07	324	135	406	188	0.46

Case 4, values in (MPa).

N_f	$\overline{AC}$ Pure shear amplitude	$\overline{AB}$ Shear amplitude	$\overline{AD}$ Axial amplitude	$\overline{BC}$ Shear increment	ssf
1.E+03	567	375	650	192	0.30
1.E+04	493	323	558	171	0.31
1.E+05	428	277	480	151	0.32
1.E+06	372	238	412	134	0.33
1.E+07	324	204	354	119	0.34

Case 5, values in (MPa).

N_f	$\overline{AC}$ Pure shear amplitude	$\overline{AB}$ Shear amplitude	$\overline{AD}$ Axial amplitude	$\overline{BC}$ Shear increment	ssf
1.E+03	567	508	508	59	0.12
1.E+04	493	389	389	104	0.27
1.E+05	428	298	298	131	0.44
1.E+06	372	228	228	144	0.63
1.E+07	324	175	175	149	0.85

A.2 Axial and shear fatigue trend lines from fatigue failure results for loading cases shown in figure 3.1.

Case	$sar = \frac{\tau_a}{\sigma_a}$	Trend line (MPa)	R^2
1	0	$\sigma_a = 1204.3(N_f)^{-0.071}$ $\tau_a = 0$	0.87
2	∞	$\sigma_a = 0$ $\tau_a = 864.78(N_f)^{-0.061}$	0.99
3	0.33	$\sigma_a = 938.81(N_f)^{-0.052}$ $\tau_a = 312.94(N_f)^{-0.052}$	0.85
4	0.58	$\sigma_a = 1025.7(N_f)^{-0.066}$ $\tau_a = 592.3(N_f)^{-0.066}$	0.96
5	1	$\sigma_a = 1132.5(N_f)^{-0.116}$ $\tau_a = 1132.5(N_f)^{-0.116}$	0.86